https://doi.org/10.5194/hess-2023-31
Preprint. Discussion started: 2 February 2023
© Author(s) 2023. CC BY 4.0 License.

Hydrology and Earth System Sciences
Discussions

Understanding the Compound Flood Risk along the Coast of the Contiguous United States

Dongyu Feng[1], Zeli Tan[1], Donghui Xu[1], L. Ruby Leung[1]

[1]Atmospheric Sciences and Global Change Division, Pacific Northwest National Laboratory, Richland, WA, 99354, USA

Correspondence to: Zeli Tan (zeli.tan@pnnl.gov)

Abstract. Compound flooding is a type of flood events caused by multiple flood drivers. The associated risk has usually been assessed using data-based statistical analyses or physics-based numerical models. This study proposes a compound flood (CF) risk assessment (CFRA) framework for coastal regions in the contiguous United States (CONUS). In this framework, a large-scale river model is coupled with a global ocean reanalysis dataset to (a) evaluate the CF exposure risk related to the coastal backwater effects on river basins, and (b) generate spatially distributed data for analyzing the CF hazard risk using a bivariate statistical model of river discharge and storm surge. The two kinds of risk are also combined to achieve a holistic understanding of the continental-scale CF comprehensive risk. The estimated CF risk shows remarkable inter- and intra-basin variabilities along the CONUS coast with more variabilities in the CF hazard risk over the US West and Gulf coastal basins. Different risk assessment methods present significantly different patterns in a few key regions, such as San Francisco Bay area, lower Mississippi River and Puget Sound. Our results highlight the needs to weigh different CF risk measures and avoid using single data-based or physics-based CFRAs. Uncertainty sources in these CFRAs include the use of gauge observations, which cannot account for the flow physics or resolve the spatial variability of risks, and underestimations of the flood extremes and the dependence of CF drivers in large-scale models, highlighting the importance of understanding the CF risks for developing a more robust CFRA.

Keywords: compound flood, coastal flood, flood risk assessment, uncertainty analysis, river model

1 Introduction

Compound flooding is a type of multivariate flood events when various flood drivers occur concurrently in the same or adjacent regions (Santiago-Collazo et al., 2019). Specifically, over coastal regions, compound flooding is generally driven by fluvial and coastal processes. While an individual driver may not be extreme, the complex nonlinear interactions between fluvial and coastal processes can intensify the joint impact of multivariate drivers (Dykstra & Dzwonkowski, 2020), causing significant flood hazards (Mehran et al., 2017; AghaKouchak et al., 2018) and negative socio-environmental impacts (Hinkel et al., 2014; Wahl et al., 2017). It is possible that a compound flood (CF) event is not caused by extreme weather (Couasnon et al., 2020) but rather occurs when the associated drivers exceed their respective thresholds (Zscheischler et al., 2020).

Assessing CF caused by co-occurring fluvial and coastal flooding is important for low-lying coastal regions where 680 million people live globally and this number is projected to increase to over 1 billion by 2050 (Pörtner et al., 2019). Such flood hazard is intensified during “wet” storms by simultaneous rainfall and storm surge events and can be exacerbated by future sea level rise (Kulp and Strauss, 2019) and climate change (Bevacqua et al., 2019; Gallien et al., 2018; Gori & Lin, 2022). To mitigate the CF risks, it is crucial to understand the driving processes and the related uncertainties in the risk assessment.

Compound flood risk assessment (CFRA) is critical for flood planning, management, timely emergency response and decisions. CF risk has substantial spatial variabilities since the CF drivers and the CF risk dependence on the drivers are affected by the local conditions (Wahl et al., 2015), such as the characteristics of local basins that affect runoff generation, river routing (Hendry et al., 2019), synoptic weather systems, and storm characteristics (Seneviratne et al., 2012).

At the regional scale, data-based CFRAs are used to assess the CF hazard risk which is defined as the frequency of a CF event. The CF hazard risk is usually represented by statistical dependence or co-occurrence rate of multiple flood drivers including discharge and surge (Moftakhari et al., 2017; Sadegh et al., 2018; Muñoz et al., 2020); precipitation and surge (Bevacqua et al., 2019); discharge, surge, and wave (Camus et al., 2021), etc. Data-based CFRAs perform statistical analyses using long-term data at paired gauges near the land-ocean interface. The data can be obtained either from large-scale numerical simulations (Eilander et al., 2020; Nasr et al., 2021) or gauge observations (Ward et al., 2018; Paprotny et al., 2020). Bivariate or multivariate analyses are performed to examine the dependence structure among flood drivers (Nasr et al., 2021; Salvadori et al., 2007; Zscheischler et al., 2020) and joint exceedance probability when all drivers are above their predefined thresholds, e.g., 95th or 99th percentile (Kew et al., 2013, Salvadori et al., 2016).

Data-based CFRAs can reveal critical regional variability in terms of the strength of individual drivers, their dependence structures, and joint occurrence, as well as the CF hotspots. Gauged observations provide a robust basis for large-scale risk assessments (Couasnon et al., 2020). The simple structure in statistical models facilitates the investigation of major CF drivers. However, the variability of CF risks is limited to the gauge level since data of the entire river basin is often not available. Consequently, the physical processes behind flood drivers and the influence of local basin characteristics and river topology cannot be fully explored.

CF risk can vary substantially across rivers and estuaries (Xiao et al., 2021; Zhang et al., 2020) as a result of the impact of river topology and tidal variations (Bakhtyar et al., 2020; Gori et al., 2020) and the characteristics of drainage basins that regulate the river processes (Dykstra & Dzwonkowski, 2021). For example, river topology controls streamflow routing and backwater propagation through river networks (Bilskie & Hagen, 2018). Even if the data-based CFRA yields a high probability of CF event in a region, the CF exposure can be limited by a steep channel slope because the coastal backwater is not able to propagate upstream. Thus, the physical processes can influence the results of CFRA. Physics-based CFRAs have been applied to measure the population and property exposure to CF, i.e., the CF exposure risk, using spatially abundant observations (Dykstra & Dzwonkowski, 2020; Valle-Levinson et al., 2020), numerical models (Kumbier et al., 2018; Lian et al., 2013; Olbert et al., 2017; Ye et al., 2020), and the integration of both (Moftakhari et al., 2019; Muñoz et al., 2020;

Hydrology and Earth System Sciences
Open Access
Discussions

Serafin et al., 2019). However, applications of physics-based CFRAs are mostly limited to basin scales because of the computational cost of high-resolution numerical models.

Recent developments in large-scale river models (Feng et al., 2022; Ikeuchi et al., 2017; Luo et al., 2017) and global water level and storm surge reanalysis datasets (Muis et al., 2017, Muis et al., 2020) facilitate physics-based CFRA across rivers and estuaries. Large-scale river models can capture streamflow at fine temporal scales (Towner et al., 2019) and resolve backwater effects when coupled with the tide and surge induced water level (Feng et al., 2022; Muis et al., 2020). Such models offer an appropriate tool to evaluate spatially-varied flood drivers, flood extent and population exposure from basin to global scales over multiple decades.

The CF hazard risk and exposure risk evaluated separately by the aforementioned data-based or physics-based CFRAs may produce inconsistent results (K. Xu et al., 2022). The risk determined based on either CFRA can cause biased judgments. For example, for high-gradient and sparsely populated regions, high CF hazard risk will not result in high CF exposure risk. Instead of advocating for either method, this study proposes a CFRA framework that analyzes both hazard and exposure risks, as well as the CF comprehensive risk that combines the two types of risks (Kron, 2005). We identify the strengths and limitations of each framework and highlight the possible uncertainties within the CFRA framework.

A robust CFRA should consider the uncertainties associated with flood frequency and possible flood damages and provide a thorough understanding of the uncertainties related to the risk analysis (Apel et al., 2004). Uncertainty analysis is challenging due to various uncertainty sources and has drawn significant attention in risk assessments in the fields of coastal flooding (Hinkel et al., 2014; Vousdoukas et al., 2018; Parodi et al., 2020), fluvial flooding (Apel et al., 2004; Egorova et al., 2008), and compound flooding (Dung et al., 2015; Sadegh et al., 2017; Sadegh et al., 2018; Zhang et al., 2020).

The contiguous United States (CONUS) (Fig. 1) consists of 48 states, with coastal counties occupying about 10% of the total area. There are 17 major port cities, and ~40% of the US population residing in coastal counties are subject to high coastal flooding risks (Hanson et al., 2011). The CF hazard risk in CONUS has been assessed previously via statistical modeling for CF drivers' dependence (Wahl et al., 2015; Nasr et al., 2021) and joint probability (Moftakhari et al., 2017; Ghanbari et al., 2021) using data-based CFRAs. However, none of the existing studies have accounted for the variability in the fluvial process and river topology, the coastal backwater effects, as well as the associated uncertainty. The CF exposure risk is also poorly understood. To fill this gap, we develop a new CFRA framework based on both statistical analyses and a large-scale river model that is coupled with a global ocean model reanalysis product. We provide a holistic hazard and exposure risk assessment of the compounding fluvial and coastal flooding along the CONUS coastline, focusing on understanding the uncertainties in both data-based and physics-based CFRAs.

2 Methodology

This section describes the new CFRA framework and provides details of the statistical and river modeling approaches. We also describe the methods to identify uncertainties within the CFRA.

https://doi.org/10.5194/hess-2023-31
Preprint. Discussion started: 2 February 2023
© Author(s) 2023. CC BY 4.0 License.
Hydrology and Earth System Sciences
Discussions

2.1 The CFRA framework

The CFRA framework (Fig. 1) provides estimates of CF hazard, exposure, and comprehensive risks (Maskrey et al., 2011). The CF hazard risk refers to the temporal frequency of CF events and is derived from the bivariate statistical modeling of river discharge and storm surge. The CF exposure risk is defined as the exposed population within the CF backwater extent, which is modeled using a large-scale river model, the Model for Scale Adaptive River Transport (MOSART) (Li et al., 2013). Correspondingly, the CF comprehensive risk is the combination of the hazard and exposure risks.

MOSART is a physics-based river routing model at the basin to global scales. The model routes the total runoff from hillslope to river outlet through river networks with floodplain inundation represented using a macroscale inundation scheme (Luo et al., 2017). In this study, MOSART simulation is performed on the CONUS domain using a 1/8° grid from 1979 to 2018, with the first year excluded as model spin-up time. For more detailed descriptions of the model, please refer to Li et al., 2022. In this study, the channel slope is derived from the 15 arcsec digital elevation model (DEM) of the HydroSHEDS and river vector data (Lehner et al., 2008, Lehner & Grill, 2013). The runoff forcing is from Global Reach-level Flood Reanalysis (GRFR) (Yang et al., 2021), a bias-corrected offline simulation from a high-resolution VIC land surface model forced with precipitation from the Multi-Source Weighted-Ensemble Precipitation (MSWEP) (Beck et al., 2019) and other climatic forcings from ECMWF Reanalysis v5 (ERA5) (Hersbach et al., 2018). The downstream boundary is enforced at the river outlets for rivers with a drainage area >1000 km^2 (169 in total). We apply two types of boundary condition (BC): (1) Time-varying storm surge (SS) level obtained from the third-generation Global Tide and Surge Model (GTSM) (Muis et al., 2022), and (2) fixed mean sea level (MSL). For small river basins, we apply the normal depth boundary at their outlets (Feng et al., 2022), which is MOSART's default setting. The GTSM is a global hydrodynamic model with a coastal resolution of ~2.5 km (~1.25 km in Europe). Driven by the ERA5 atmospheric reanalysis dataset, the GTSM produces time series of the total water level and storm surge at global coasts from 1979 to 2018 (Muis et al., 2020), which have been validated globally (Dullaart et al., 2020, Muis et al., 2020).

We run the statistical model with simulated streamflow from MOSART simulation forced by the dynamic GTSM BC. The MOSART simulated streamflow is validated at 61 USGS gauges (Fig. 2), which are selected based on the following criteria: (1) These gauges are located at the mainstem of the rivers and within 80 km of the corresponding river outlets; (2) the corresponding river reaches have upstream drainage areas larger than 1,000 km^2; and (3) the gauge data have a temporal coverage longer than 10 years. The MOSART accuracy is evaluated using Kling-Gupta efficiency (KGE) (Gupta et al., 2009) and coefficient of determination (r^2). MOSART shows reasonable accuracy in simulating daily streamflow (Fig. S1), with both r^2 and KGE generally over 0.6. The model performance is lower at a few gauges, likely caused by the coarse grid resolution (1/8°), approximations of river geometry in MOSART, and uncertainty in the GRFR runoff data. The GTSM simulated water level along the CONUS coastline is validated against the NOAA measurements at 34 tidal gauges (Rashid et al., 2019) that have 80% or more data available over the simulation period (Fig. 2). The GTSM modeled water level achieves

https://doi.org/10.5194/hess-2023-31
Preprint. Discussion started: 2 February 2023
© Author(s) 2023. CC BY 4.0 License.
Hydrology and Earth System Sciences
Discussions

satisfactory performance along the CONUS coast when measured by r^2 and root mean squared error (RMSE) (Fig. S2): r^2 is generally over 0.75 and RMSE is below 0.5 m. There are only two exceptions on the East coast with either low r^2 or high RMSE, because the GTSM grid of the two gauges does not resolve the corresponding estuaries. Overall, the MOSART and GTSM model results are adequate for our goals which are to construct a new CFRA framework at the continental scale and study the associated uncertainties (Towner et al., 2019).

The CF hazard risk is derived from the bivariate statistical modeling. The analysis is performed for the MOSART coastal cells which are defined as the grid cells within seven upstream cells from the corresponding river mouths. It is assumed that coastal processes have no impacts on the regions beyond this extent. The simulated daily streamflow (Q) at each selected cell is paired with the coastal storm surge (SS) level from the GTSM reanalysis dataset at the grid cell nearest to the outlet. The CF hazard risk is calculated by the following procedure:

(a) storm surge event selection: identifying the extremes using the peak-over-threshold (POT) method and using an event selection scheme to extract all SS events with the SS level over 95th percentile of the corresponding station (Feng et al., 2022);

(b) univariate analysis: fit the selected SS and Q into their marginal distributions and calculate the marginal exceedances, i.e., the probability of exceeding the 95th percentile of the respective marginal distributions;

(c) dependence assessment: determine if the bivariate variables are dependent of each other based on Kendall's rank correlation coefficient (τ) (Kendall, 1938);

(d) bivariate analysis: calculate the joint exceedance probability based on the marginal distributions and the dependence structure.

As the first step, the event selection only samples positive SS from the time series data, which facilitates the fitting of marginal distributions. The threshold of 0.95 ensures that at least 50 pairs of Q and SS data points are available for bivariate modeling. The occurrence probability of the storm surge events ($P(SS)$) is calculated for each river basin as the ratio of the duration of all SS events divided by the simulation period.

In the univariate analysis, the marginal distributions of Q and SS (f_Q and f_{SS}) are selected based on the AIC (Akaike Information Criterion) statistics from 8 candidate distributions: Gamma, Generalized Pareto, Pearson Type III, Lognormal, Generalized Extreme Value, Generalized Logistic, Log-gamma and Gumbel. The fitted distributions are tested using the Kolmogorov-Smirnov and chi-square tests for goodness of fit. The marginal exceedance probabilities of Q and SS (P_Q and P_{SS}) are

$$P_Q = F_Q(q^*), \tag{1}$$

$$P_{SS} = F_{SS}(ss^*), \tag{2}$$

where q^* and ss^* represent the 95th percentile values.

The dependence between Q and SS is assessed for each MOSART cell by calculating the Kendall's correlation (τ). The significance level is set as 0.05. We consider Q and SS to be dependent of each other when they display a significant positive

https://doi.org/10.5194/hess-2023-31
Preprint. Discussion started: 2 February 2023
© Author(s) 2023. CC BY 4.0 License.

correlation (p-value<0.05). Although assessed in extensive CF literature, the dependence structure alone does not represent the CF hazard risk. For example, in a case when Q and SS are highly dependent, the CF risk can still be low if both drivers do not show frequent extremes. Thus, the joint exceedance probability is calculated based on the "AND" hazard scenarios (Salvadori et al., 2016), which assumes both Q and SS exceed their corresponding thresholds.

The joint exceedance probability ($P_{Q,SS}$) is given as

$$P_{Q,SS} = 1 - F_Q(q^*) - F_{SS}(ss^*) + F_{Q,SS}(q^*, ss^*), \qquad (3)$$

where $F_{Q,SS}$ is the cumulative joint distribution which is a function of the cumulative marginal distributions, F_Q and F_{SS}. When Q and SS are independent, $F_{Q,SS}(q^*, ss^*)$ is simply the product of the marginal exceedance probability:

$$F_{Q,SS}(q^*, ss^*) = F_Q(q^*) \cdot F_{SS}(ss^*). \qquad (4)$$

When Q and SS are dependent, the joint distribution is expressed using a copula function as (Grimaldi & Serinaldi, 2006):

$$F_{Q,SS}(q^*, ss^*) = C_{Q,SS}(F_Q(q^*) \cdot F_{SS}(ss^*)), \qquad (5)$$

where $C_{Q,SS}$ is the bivariate copula function that allows the analytical formulation of the dependence structure. For each MOSART cell where Q and SS are dependent, the copula function is selected based on AIC from 24 candidates (Moftakhari et al., 2017) using an R-package (Kojadinovic & Yan, 2010). The selected copula function is then tested using the Cramer-von Mises goodness-of-fit test. The marginal exceedance probabilities (P_Q and P_{SS}) and their joint exceedance probability ($P_{Q,SS}$) are conditioned on the occurrence of the storm surge events as they are calculated from the SS data sampled in Step (a). These probabilities are multiplied by $P(SS)$ to obtain the unconditional probabilities.

The CF exposure risk is defined as the accumulated population (W_p) over the coastal backwater flooded region during CF events when $Q > q^*$ and $SS > ss^*$. To calculate W_p, we use the 1000-m resolution Global Human Settlement Layer (GHSL) population data that is updated every five years from 1975 to 2020 (Schiavina et al., 2019). We aggregate the data to the 1/8° MOSART grid and linearly interpolate the data over the simulation period. The backwater flooded fraction caused by CF is identified by comparing the simulations with the two different downstream BCs:

$$\Delta f(t, i) = f_{GTSM}(t, i) - f_{MSL}(t, i), \qquad (6)$$

where f represents the simulated flooded fraction of each grid cell, t is the model output time step during CF and i is the grid cell index of the MOSART coastal cells. During a single CF event, human exposure in a grid cell is the product of the corresponding population and Δf. Thus, the CF exposure risk is the accumulated human exposure over all CF events during the simulation period.

The CF comprehensive risk is represented by a risk index ($CFRI$), defined as the product of the CF exposure risk and the CF hazard risk (Judi et al., 2018; Kalyanapu et al., 2015; Phongsapan et al., 2019):

$$CFRI = 10 \times CFHI \times CFEI, \qquad (7)$$

where 10 is the scaling factor that upscales the risk index to better visualize the results, and the CF hazard index ($CFHI$) and the CF exposure index ($CFEI$) are obtained by normalizing $P_{Q,SS}$ and W_p with their corresponding 95th percentile values. We do not use the maximum value as the normalizing constant because the maximums can be too extreme and likely

© Author(s) 2023. CC BY 4.0 License.

concentrates on the river outlets where $CFEI$ is high. The use of such a normalization would shadow the $CFRI$s at upstream regions. Our approach transforms the probability of occurrence into a direct measure of human exposure. However, it should be noted that the combination of different types of risks, despite providing a comprehensive estimation of the CF risk, is subjective and may affect the risk assessment results.

2.2 Uncertainty analysis in CFRA

In this section, we investigate the uncertainty sources in the large-scale CFRAs. Then, we examine the spatial variability in streamflow and storm surge and the relative impacts of riverbed elevations on the physics-based CFRA. The uncertainties in the data-based and physics-based CFRAs are also assessed by comparing the risk estimates at paired observation gauges. While it is challenging to accurately quantify such uncertainties in the CFRAs, we aim to highlight the significance of different uncertainty sources.

2.2.1 CFRA uncertainty sources

The uncertainty in CFRA can generally be classified into epistemic uncertainty and aleatory uncertainty. Aleatory uncertainty is inherent to the intrinsic variability in natural and anthropogenic systems (Hall, 2003). Epistemic uncertainty is due to limited knowledge of natural systems and can be reduced with an improved understanding of the systems (Ferson & Ginzburg, 1996; Uusitalo et al., 2015). Herein we list and classify the possible uncertainty sources in the CFRA (Table 1). This classification may be subjective because sometimes the distinction between incomplete knowledge of the systems and natural variabilities cannot be easily identified (Apel et al., 2004).

In data-based CFRAs, aleatory uncertainties are related to the spatial variabilities of the fluvial processes and river topology that are not well represented in gauge data (Fan et al., 2021) and the stationary assumption of statistical models (Ghanbari et al., 2021). It is widely known that the CF risk is nonstationary due to the changing climate. Additionally, the flood drivers vary significantly depending on the local topology (Sun et al., 2021), which is usually not accounted for in data-based CFRAs. The timing of peak floods changes from an upstream gauge to the outlet and the storm surge varies between an offshore tidal gauge and the river mouth. Although the data-based CFRAs use a time window of 1~5 day (Ward et al., 2018; Wu et al., 2021) to account for this time lag, this procedure inevitably increases the possibility of falsely matching two independent events when distant observation gauges are used. Epistemic uncertainties in statistical models can include measurement errors and model structure uncertainty. Although the errors of the water level measurements at National Oceanic and Atmospheric Administration (NOAA) tidal gauges are usually small (O(1mm)) (Asher et al., 2019), the quality of the U.S. Geological Survey (USGS) measured streamflow varies significantly. For example, it was found that the USGS streamflow errors can reach over 8% (Turnipseed & Sauer, 2010), and be even much larger during extreme events as the measurements are not sufficiently continuous to cover many extremes (Kiang et al., 2018). Moreover, USGS gauges may not be installed exactly at the river-ocean interface, which cannot capture the river discharge to the ocean. The statistical analysis of CF risks based on these measurements will inevitably be biased. Moreover, model structure uncertainties always exist in

© Author(s) 2023. CC BY 4.0 License.

statistical models, such as the selection of marginal distribution functions and dependence models. The latter is critical for computing the joint exceedance probability of CF (Fan et al., 2021).

Numerical models used in both data-based and physics-based CFRAs also have many uncertainties. Intrinsically, there is uncertain climate change that modifies climatological and societal systems (Bouwer, 2013). For numerical models, the epistemic uncertainty can be classified into uncertainties in model parameters, structure, and input data. The parameter uncertainty and the data uncertainty are caused by uncertain model parameters (e.g., channel roughness coefficient), uncertain river topology, and channel geometry, respectively. In large-scale river models, the hydraulic physics are usually simplified to guarantee computational efficiency, such as using an empirical formulation of floodplain inundation (Yamazaki et al., 2012), approximations in flood wave physics (Hodges, 2013). In addition, coarse mesh resolutions used by large-scale river models can cause unresolved river networks and topology (Parodi et al., 2020). All these uncertainties could be related to inaccurate assessments of the event extremes (Muis et al., 2017) and flood drivers' dependence (Nasr et al., 2021).

2.2.2 Impact of riverbed elevation

The riverbed elevation determines the extent of coastal backwater propagation. To understand its impacts on CF risks, a random forest analysis (Breiman, 2001) is performed to evaluate the relative importance of riverbed elevation against Q and SS to the backwater effects.

Random forest models are widely used to assess the relative importance of predictors with respect to a response variable (Breiman, 2001; Woolway et al., 2021). Here, the predictor variables are Q, SS and the riverbed elevation. For each coastal grid cell, we use the MOSART simulated Q, the GTSM simulated SS at the river outlet, and the grid cell elevation. The response variable is the backwater-induced water volume change (ΔV):

$$\Delta V(t,i) = \big(h_{GTSM}(t,i) - h_{MSL}(t,i)\big)L(i)W(i) + \big(fv_{GTSM}(t,i) - fv_{MSL}(t,i)\big), \tag{8}$$

where h is the channel water depth at the i-th grid cell and the time t, L is the main channel length of the i-th cell and W is the corresponding width, and fv is the floodplain water volume. The predictor and response variables are normalized to [0,1] before fitting into the random forest model. We fit independent random forest models for every coastal river basin, with sizes varying from ~10 grid cells to >100 cells.

2.2.3 Impact of fluvial processes

The impact of complex fluvial processes on streamflow is significant. The shift in streamflow peaks from an upstream location to the river outlet will cause biases in the CFRA if the upstream Q measurements are used in the CF risk analysis. To identify the associated uncertainty, we compute the time-averaged shift of modeled Q or SS peaks between the observation gauges and the corresponding river outlets over the simulation period. The calculation of the shift in peaks includes the following steps: (i) for a USGS or NOAA gauge, we first locate the MOSART or GTSM grid cell nearest to the corresponding river outlet and extract the Q or SS extreme events of the grid cell; (ii) we then identify the peak date of each

https://doi.org/10.5194/hess-2023-31
Preprint. Discussion started: 2 February 2023
© Author(s) 2023. CC BY 4.0 License.
Hydrology and Earth System Sciences Discussions
Open Access

extreme event and define a time window of ±5 days; (iii) over the defined time window, we search for the date of the peak simulated Q or SS at the MOSART or GTSM grid cell where the USGS or NOAA gauge is located and calculate the difference between the two peak dates. If no peaks are identified for the gauge grid cells, we assume that the difference is five days.

We also compute the flow time over the river basins, defined as the time that terrestrial runoff takes to travel from an upstream cell to the outlet via the river network. The flow time is determined by the basin characteristics, such as channel geometry, meandering and riverbed elevation. A longer flow time typically implies a larger time shift in streamflow peaks. In this study, the calculated flow time of each grid cell is averaged over the simulation period.

2.2.4 Model-data comparison

Lastly, we also evaluate the uncertainty caused by using measured versus modeled Q and SS for analysis. For this, we compare the statistical metrics of P_Q, P_{SS}, τ and $P_{Q,SS}$ for the modeled and measured pairs of Q and SS at 24 river basins (Table S1), where a USGS gauge paired with a neighboring NOAA tidal gauge can be found. We consider three combinations of Q and SS: a) MOSART modeled Q and GTSM modeled SS at the river outlet, b) MOSART modeled Q at the USGS gauge and GTSM modeled SS at the NOAA gauge, and c) USGS measured Q and NOAA measured SS. The comparison between the combinations (a) and (c) represents the uncertainty due to fluvial processes and river topology. The comparison between the combinations (b) and (c) represents the uncertainty from the numerical modeling.

3 Results

3.1 Uncertainty in CFRA

3.1.1 The relative importance of riverbed elevation

Our result shows the crucial role of the riverbed elevation in determining the CF risks in the river basins, which contrasts with previous studies that mostly focused on the dynamics of Q and SS (Fig. 3). In particular, the elevation effect dominates in the Northwest coast (Fig. 3a), where the large elevation gradient of the riverbed impedes the propagation of coastal backwaters so the areas of high CF risks are restricted to the coastline. In the other regions, the relative importance of Q and SS varies, which also depends on the riverbed elevation. The SS impact is limited along the West coast due to the elevated river channels but exceeds the impact of Q in the low-lying East and Gulf coasts (Fig. 3d). The importance of the riverbed elevation to CF risks identified in this study is consistent with findings from some local studies (Bilskie & Hagen, 2018, Gori et al., 2020). In brief, the relative importance of the CF drivers varies depending on local basin characteristics.

https://doi.org/10.5194/hess-2023-31
Preprint. Discussion started: 2 February 2023
© Author(s) 2023. CC BY 4.0 License.

3.1.2 Shift in peaks

The shifted peak days in Q and SS from the USGS or NOAA gauges to the corresponding river outlet show that the data-based CFRA may have large uncertainties (Fig. 4). The averaged time shift in the Q peaks varies from 1 to 5 days, depending on the local topology. In the northwestern and northeastern river basins, where the elevation gradient is large, the flow time is ~ 1 day and the resulting shifts are small (~ 1$\pm$1 day). In contrast, the shifts and the flow time are much larger (~ 3$\pm$1 days) in the low-gradient regions of the East and Gulf coasts. The time shifts in the SS peaks generally depend on the distance between the tidal gauges and river mouth. In CONUS, the shifts are generally small (~ 1 day) with lower variabilities. Our results show that the combined shifts in the peaks of the two flood drivers in some locations can be greater than five days, a duration used by many previous studies as the time window to identify extreme CF events (Ward et al., 2018; Wu et al., 2021).

3.1.3 Model-data comparison

We compare the marginal exceedance probabilities of discharge and storm surge (P_Q and P_{SS}), the Kendall's rank correlation coefficient (τ) and the joint exceedance probability ($P_{Q,SS}$) computed from the three combinations of Q and SS described in Section 2.2.3 at 26 river basins (Fig. 5). For the same river basin, these statistical metrics can differ significantly among the combinations, indicating substantial uncertainties due to fluvial processes and river topology, as well as from the numerical modeling. Generally, P_{SS} is more consistent among the three combinations, because the time shifts in the SS peaks are small (Fig. 4). In contrast, P_Q, τ and $P_{Q,SS}$ show greater variations.

There are significant differences of P_Q, τ and $P_{Q,SS}$ between the combinations of the modeled Q and SS at the interface and at the observation gauges, particularly in the West coast (black vs. blue bars in Fig. 5). As discussed in Section 2.2.3, this indicates the spatial variabilities of the CF risk within the river basins and the associated uncertainty in the data-based CFRA. The uncertainty in $P_{Q,SS}$ varies along the CONUS coast and is more distinct in several basins (e.g., 14243000 and 11530500) due to the larger variability in P_Q and higher τ.

There are also significant differences of P_Q, τ and $P_{Q,SS}$ between the combinations of modeled and measured Q and SS at observation gauges across all CONUS coasts (blue vs. red bars in Fig. 5). As mentioned in Section 2.2.3, the differences indicate the uncertainty within the numerical models that could influence the assessment of the CF risk. The values of P_Q and P_{SS} calculated from the modeled Q and SS are generally smaller than those calculated from observations. This is likely because the MOSART and GTSM models underestimate the Q and SS extremes, a well-known uncertainty in large-scale models (Muis et al., 2017; Yang et al., 2021). It should be noted that the USGS reported streamflow peaks are likely uncertain because USGS derives streamflow based on the stage-discharge relationship, but the data used for the derivation are rarely collected during extreme events (Turnipseed & Sauer, 2010). Besides the uncertainties mentioned above, we find that the use of modeled Q and SS could lead to underestimation of the dependence (τ) and thus the joint risk ($P_{Q,SS}$),

Hydrology and Earth System Sciences
Open Access
EGU
Discussions

particularly in the West and Northeast coasts (Fig. 5). The uncertainties in P_Q and τ are more important in determining the uncertainty in $P_{Q,SS}$ in the West and East coasts, respectively.

We provide a few example basins to demonstrate the various types of uncertainties (Figs. S3-S7). Figures S3 and S4 show the epistemic uncertainty caused by inappropriate in-situ locations. In Figure S3, the streamflow measured at the tributary of a mainstem is much lower and cannot represent the river discharge at the outlet. In Figure S4, SS has a different probability distribution than that modeled at the river-ocean interface. Gauge 9419750, despite being close enough to the river outlets, is blocked by man-made barrier islands, thus presenting a different SS signal. Figure S5 shows the aleatory uncertainty due to the variability in Q between the USGS gauge and the river outlet. While the probability distributions of Q and SS are similar among the three cases, Q at the upstream gauge typically yields smaller peaks in correspondence to the SS peaks, resulting in lower τ. The epistemic uncertainties in Figures S6 and S7 are caused by the GTSM and MOSART models, respectively. In both examples, the dependence between Q and SS is underestimated because GTSM and MOSART underestimate the peaks in SS and Q, respectively. In particular, the MOSART performance is poor in Figure S7, which yields a different Q distribution.

The uncertainty analyses underscore the uncertainties in both data-based and physics-based CFRAs, which should be made aware of in applications. Importantly, while the uncertainty in the physics-based CFRA may be reduced by improving the numerical models, it is not possible for the data-based CFRA to account for the physical processes and the variability at the basin scale, such as the varied streamflow and backwater propagation extent.

3.2 CFRA

This section shows the CFRA framework that provides spatially distributed CF risk estimates based on the modeled Q and SS and captures the impacts of fluvial processes and riverbed elevation. The CF comprehensive risk combines the CF hazard risk derived from statistical models and the CF exposure risk simulated by the coupled MOSART and GTSM.

3.2.1 CF hazard risk

The CF hazard risk is represented by the joint exceedance probability of Q and SS ($P_{Q,SS}$), which depends on their respective marginal exceedance probability (P_Q and P_{SS}) and the dependence structure (Fig. 6). The spatial map shows larger P_Q variations in the West and Gulf coasts but a more uniform P_Q pattern in the East coast. The highest P_Q (~ 3.0%) is observed in the Northwest coast (Fig. 6), where the corresponding P_{SS} is low (~ 1.0%). The variability in P_{SS} is much smaller compared to that of P_Q. The values of P_{SS} are high (~ 2.0%) in the western Gulf coast in correspondence with the moderate P_Q of the same basins (~ 2.5%). Moreover, P_Q shows critical intra-basin variability within several basins, with a standard deviation of up to 1%. The marginal probability provides the basis to derive the drivers' dependence structure, copula functions, and joint probability.

https://doi.org/10.5194/hess-2023-31
Preprint. Discussion started: 2 February 2023
© Author(s) 2023. CC BY 4.0 License.

The result of the Kendall's rank correlation coefficient (τ) shows large inter- and intra-basin variabilities of τ in CONUS (Fig. 7). The highest dependence is observed along the Northwest coast, where τ is approximately 0.2. The other coastal regions generally have a lower τ (0~0.1) and the τ value normally decreases upstream within the river basins. The intra-basin variability of τ is the greatest in the West coast.

Lastly, we compute $P_{Q,SS}$ for the river basins along the CONUS coast (Fig. 8). The value of $P_{Q,SS}$ shows larger variabilities than that of P_Q, P_{ss} and τ as it includes uncertainties in the marginal distribution and dependence structure as well as uncertainty of the copula function selection. The highest $P_{Q,SS}$ (~0.4%) is observed in the Northwest and Gulf coasts, while that in the East coast is generally less than 0.3%. The greater variability of $P_{Q,SS}$ in the West and Gulf coast basins is consistent with the spatial pattern of the marginal exceedance probability and dependence (Figs. 6 and 7). Interestingly, in several basins (Fig. S8), $P_{Q,SS}$ differs significantly between the mainstem and tributaries.

3.2.2 CF exposure risk

The cumulative population exposed to CF over the simulation period is computed to represent the CF exposure risk (Fig. 9). The human exposure to CF varies from 0 to 10,000 people and is restricted to the coastline. This is not unexpected because the CF-impacted riverine regions are governed by the river topology and the amplitude of SS at the river outlets. Overall, this CF exposure risk is low because (a) the backwater extent is limited to the low-gradient regions, and (b) the occurrence of CF events is low over the 40-year period. Although the CF exposure for the West coast is only observed at the river outlets because of the large riverbed elevation impact (Fig. 7), it can extend several cells (O(10^4 m)) upstream in several river basins of the East and Gulf coasts. Also, the CF exposure risk has a spatial variability very different from the CF hazard risk, for example in the Northwest coast. These findings demonstrate the necessity to account for the impacts of river topology and calculate spatially distributed risks in CFRA.

3.2.3 CF comprehensive risk

The CF comprehensive risk is derived based on the CF hazard and exposure risks (Fig. 10). The CF comprehensive risk varies significantly along the CONUS coast and is the highest at the river outlets although the risk can be present to a much larger extent over most river basins of the East and Gulf coasts due to the upstream propagation of backwaters. This pattern is consistent with the flood exposure risk. In a few low-lying regions of the East and Gulf coasts, the CF risk extends several cells upstream from the river-ocean interface. In addition, we identify a few hotspots ranked using the $CFRI$ averaged over a river basin (Table 2). Table 2 shows that the coastal area of San Joaquin River and Hudson River where Silicon Valley and New York City are located, respectively, are particularly vulnerable to CF. The total exposed population and the maximum exceedance probability ($P_{Q,SS}$) are also provided. Although the three metrics correspond to different types of CF risks, these hotspots require extra attention in CF management. They also provide target regions where the computational mesh should be refined to improve model accuracy. Overall, the comprehensive risk accounts for the occurrence rate of CF events, the

https://doi.org/10.5194/hess-2023-31
Preprint. Discussion started: 2 February 2023
© Author(s) 2023. CC BY 4.0 License.
Hydrology and Earth System Sciences
Discussions
Open Access

impacts of basin characteristics and population density. The proposed CFRA avoids the biased risk estimation made by either data-based or physics-based CFRA alone and can capture the minimum risk from their respective aspect.

4 Discussions

4.1 Differences between CFRAs

We examined the CF risk along the CONUS coast using different approaches based on the co-occurrence probability of a fluvial flood and a storm surge event, the human exposure to the CF events, as well as their combined impacts. The comparison shows that the different CFRA approaches result in significantly different CF risk estimates. The difference is remarkable in a few key regions. For example, in the San Francisco Bay area, while the CF hazard risk is low, the CF exposure risk is high due to the dense population and flat topology. In contrast, although the lower Mississippi River basin is endangered by backwater flooding, the probability of a CF event is low over the 40-year period. The difference in the estimated risks could be partially explained by whether more detailed physical processes and topological factors are considered. However, the CF comprehensive risk is also valuable. For example, we find that although the Northwest coast (e.g., Puget Sound) has a high CF hazard risk, such risk is only restricted to the coastline and does not extend to the upstream regions. In summary, CFRA should not rely on any single method; more comprehensive thinking is needed considering the different characteristics among the different risk types.

The proposed CFRA also draws attention to the CF risk in upstream river basins which are usually ignored in the large-scale data-based CFRA. Typically, the flood risks related to coastal hazards (e.g., storm surge) are limited to the land-ocean interface. However, through the river networks, the backwater effects can propagate upstream by hundreds of kilometers in low-lying watersheds (Lamb et al., 2012). Our results show the CF risks extending upstream over several river basins (Fig. 9 and 10). Considering climate change impacts, we expect the CF risk will move further upstream due to the elevated sea level (Kulp and Strauss, 2019) and more frequent storm surge events (Camelo et al., 2020).

4.2 Limitations and Future work

The CFRA framework provides an effective tool to support large-scale CF risk management in CONUS. However, this study has a few limitations that warrant further improvements. First, the 40-year time series is relatively short for deriving robust extreme statistics, as extreme events can have much longer return periods (Apel et al., 2004). This type of epistemic uncertainty can be reduced by using data that covers a longer period. The simulation period is determined by the available large-scale runoff forcing (Yang et al., 2021) and the GTSM reanalysis dataset (Muis et al., 2022). Thus, long-term forcing dataset is desired for the CF modeling and analysis. Second, we only consider two CF drivers and neglect their complex interactions. The storm surge-induced backwater effects are prescribed by the time series at the MOSART boundary. However, the actual CF is driven by the interactive processes between multiple drivers, including precipitation, land surface runoff and inundation, river discharge and coastal storm surge and wave (Nasr et al., 2021). Such interactions can be

https://doi.org/10.5194/hess-2023-31
Preprint. Discussion started: 2 February 2023
© Author(s) 2023. CC BY 4.0 License.
Hydrology and Earth System Sciences
Discussions

simulated using Earth System Models (ESMs) with fully coupled land, river and ocean modeling components. Interactive coupling has been developed within the Energy Exascale Earth System Model (E3SM) (Feng et al., 2022; D. Xu et al., 2022) for further CFRA developments. Third, the MOSART simulated floodplain inundation could be a sensitive factor when estimating the CF exposure risk, as MOSART employs a macro-scale inundation scheme (Luo et al., 2017) and the model has limited resolution for evaluating risk in high population density areas. Validation of the floodplain inundation over coastal river basins is challenging because the CF inundation data is limited and such data does not differentiate coastal inundation and river floodplain inundation. Last but not least, the uncertainty sources identified in this study are undoubtedly only “the tip of the iceberg”. There are many other uncertainties related to parameterization and structural errors of data and physical models. For example, the 1/8° MOSART grid is appropriate for continental-scale multi-decadal simulations. The mesh resolution is insufficient to resolve the distributed risk within a grid cell, as neither human residence nor topology can be resolved to represent the flood exposure. The input data, such as surface runoff and digital elevation models (DEMs), have uncertainties that should be quantified. This is a well-acknowledged challenge in large-scale modeling (Cook & Merwade, 2009; Van de Sande et al., 2012).

5 Conclusion

This research proposes a CFRA framework to investigate the CF risk along the CONUS coast. This framework includes both data-based and physics-based CFRAs and assesses the CF hazard, exposure and comprehensive risks using a bivariate statistical model of river discharge and storm surge and the large-scale MOSART river model coupled with the global GTSM reanalysis dataset. The resulting CF risks show substantial variabilities at the inter- and intra-basin scales. In particular, the variability is significant in the CF hazard risk and along the West and Gulf coasts. More importantly, the three risk measures show very different spatial patterns and hotspots depending on the local settings. The high occurrence probability of a CF event does not necessarily pose high CF exposure risks. Thus, it is important to understand the different risk types and avoid biased risk estimation using either data-based or physics-based assessment methods singly. Using the new CF comprehensive risk index, we identify that the coastal area of San Joaquin River and Hudson River where Silicon Valley and New York City are located, respectively, are particularly vulnerable to CF.

Moreover, we identify the uncertainty sources in the existing CFRAs. Even though data-based CFRA is widely used in continental and global domains, the estimated CF risks based on such CFRAs could be too high because flow physics, such as complex fluvial processes and the backwater propagation, are neglected. The physics-based CFRA is more appropriate for analyzing the spatially-distributed risk but the large-scale numerical models likely underestimate the flood extremes and the dependence structure among the CF drivers. A more robust CFRA requires improved performance in large-scale modeling. In the future, we plan to apply the land-river-ocean fully coupled E3SM on a coastal-refined mesh to better represent the interactive CF physics and develop a more robust CFRA.

© Author(s) 2023. CC BY 4.0 License.

Code and data availability

The streamflow measurements are downloaded from USGS website (https://waterdata.usgs.gov/nwis) (U.S. Geological Survey, 2016). The water level observation along the CONUS coastline is obtained from NOAA tides & currents website (https://tidesandcurrents.noaa.gov/) (NOAA, 2022). The GTSM storm surge (*SS*) simulation is available from the Copernicus Climate Change Service (C3S) Climate Data Store (Yan et al., 2022). The MOSART source code and the statistical analysis code of the compound flood risk assessment are available on Zenodo (https://doi.org/10.5281/zenodo.7588256, Feng, 2023). The MOSART output and other analysis outputs can be obtained from the first author upon request.

Author contributions

DF and ZT devised the framework of the compound flood risk assessment and designed the statistical and numerical analyses. DX created the MOSART runoff forcing from the GRFR dataset. DF carried out the model simulation, risk analysis and visualization. All authors discussed and reviewed the analysis and results and contributed to the manuscript editing. ZT and LL supervised the project.

Competing interests

The authors declare that they have no conflict of interest.

Acknowledgements

The research is supported by the Earth System Model Development program areas of the U.S. Department of Energy, Office of Science, Office of Biological and Environmental Research as part of the multi-program, collaborative Integrated Coastal Modeling (ICoM) project (grant no. KP1703110/75415).

References

AghaKouchak, A., Huning, L. S., Chiang, F., Sadegh, M., Vahedifard, F., Mazdiyasni, O., Moftakhari, H., and Mallakpour, I.: How do natural hazards cascade to cause disasters?, 10.1038/d41586-018-06783-6, 2018.

Apel, H., Thieken, A. H., Merz, B., and Blöschl, G.: Flood risk assessment and associated uncertainty, Natural Hazards and Earth System Sciences, 4, 295-308, 10.5194/nhess-4-295-2004, 2004.

Asher, T. G., Luettich Jr, R. A., Fleming, J. G., and Blanton, B. O.: Low frequency water level correction in storm surge models using data assimilation, Ocean Modelling, 144, 101483, 10.1016/j.ocemod.2019.101483, 2019.

© Author(s) 2023. CC BY 4.0 License.

Bakhtyar, R., Maitaria, K., Velissariou, P., Trimble, B., Mashriqui, H., Moghimi, S., Abdolali, A., Van der Westhuysen, A., Ma, Z., and Clark, E.: A new 1D/2D coupled modeling approach for a riverine-estuarine system under storm events: Application to Delaware River Basin, Journal of Geophysical Research: Oceans, 125, e2019JC015822, 10.1029/2019JC015822, 2020.

Beck, H. E., Wood, E. F., Pan, M., Fisher, C. K., Miralles, D. G., Van Dijk, A. I., McVicar, T. R., and Adler, R. F.: MSWEP V2 global 3-hourly 0.1 precipitation: methodology and quantitative assessment, Bulletin of the American Meteorological Society, 100, 473-500, 10.1175/BAMS-D-17-0138.1, 2019.

Bevacqua, E., Maraun, D., Vousdoukas, M., Voukouvalas, E., Vrac, M., Mentaschi, L., and Widmann, M.: Higher probability of compound flooding from precipitation and storm surge in Europe under anthropogenic climate change, Science advances, 5, eaaw5531, 10.1126/sciadv.aaw5531, 2019.

Bilskie, M. and Hagen, S.: Defining flood zone transitions in low-gradient coastal regions, Geophysical Research Letters, 45, 2761-2770, 10.1002/2018GL077524, 2018.

Bouwer, L. M.: Projections of future extreme weather losses under changes in climate and exposure, Risk Analysis, 33, 915-930, 10.1111/j.1539-6924.2012.01880.x, 2013.

Breiman, L.: Random forests, Machine learning, 45, 5-32, 10.1023/a:1010933404324, 2001.

Camelo, J., Mayo, T. L., and Gutmann, E. D.: Projected Climate Change Impacts on Hurricane Storm Surge Inundation in the Coastal United States, Frontiers in Built Environment, 207, 10.3389/fbuil.2020.588049, 2020.

Camus, P., Haigh, I. D., Nasr, A. A., Wahl, T., Darby, S. E., and Nicholls, R. J.: Regional analysis of multivariate compound coastal flooding potential around Europe and environs: sensitivity analysis and spatial patterns, Natural Hazards and Earth System Sciences, 21, 10.5194/nhess-21-2021-2021, 2021.

Cook, A. and Merwade, V.: Effect of topographic data, geometric configuration and modeling approach on flood inundation mapping, Journal of hydrology, 377, 131-142, 10.1016/j.jhydrol.2009.08.015, 2009.

Couasnon, A., Eilander, D., Muis, S., Veldkamp, T. I., Haigh, I. D., Wahl, T., Winsemius, H. C., and Ward, P. J.: Measuring compound flood potential from river discharge and storm surge extremes at the global scale, Natural Hazards and Earth System Sciences, 20, 489-504, 10.5194/nhess-20-489-2020, 2020.

Dullaart, J., Muis, S., Bloemendaal, N., and Aerts, J. C.: Advancing global storm surge modelling using the new ERA5 climate reanalysis, Climate Dynamics, 54, 1007-1021, 10.1007/s00382-019-05044-0, 2020.

Dung, N. V., Merz, B., Bárdossy, A., and Apel, H.: Handling uncertainty in bivariate quantile estimation–An application to flood hazard analysis in the Mekong Delta, Journal of Hydrology, 527, 704-717, 10.1016/j.jhydrol.2015.05.033, 2015.

Dykstra, S. and Dzwonkowski, B.: The propagation of fluvial flood waves through a backwater-estuarine environment, Water Resources Research, 56, e2019WR025743, 10.1029/2019WR025743, 2020.

Dykstra, S. and Dzwonkowski, B.: The Role of Intensifying Precipitation on Coastal River Flooding and Compound River-Storm Surge Events, Northeast Gulf of Mexico, Water Resources Research, 57, e2020WR029363, 10.1029/2020WR029363, 2021.

Egorova, R., van Noortwijk, J. M., and Holterman, S. R.: Uncertainty in flood damage estimation, International Journal of River Basin Management, 6, 139-148, 10.1080/15715124.2008.9635343, 2008.

Eilander, D., Couasnon, A., Ikeuchi, H., Muis, S., Yamazaki, D., Winsemius, H. C., and Ward, P. J.: The effect of surge on riverine flood hazard and impact in deltas globally, Environmental Research Letters, 15, 104007, 10.1088/1748-9326/ab8ca6, 2020.

Fan, Y., Huang, K., Huang, G., and Li, Y.: A factorial Bayesian copula framework for partitioning uncertainties in multivariate risk inference, Environmental research, 183, 109215, 10.1016/j.envres.2020.109215, 2020.

Fan, Y., Yu, L., Shi, X., and Duan, Q.: Tracing Uncertainty Contributors in the Multi-Hazard Risk Analysis for Compound Extremes, Earth's Future, 9, e2021EF002280, 10.1029/2021EF002280, 2021.

Feng, D.: Compound flood risk analysis in CONUS, Zenodo [code], https://doi.org/10.5281/zenodo.7588256, 2023.

Feng, D., Tan, Z., Engwirda, D., Liao, C., Xu, D., Bisht, G., Zhou, T., Li, H. Y., and Leung, L. R.: Investigating coastal backwater effects and flooding in the coastal zone using a global river transport model on an unstructured mesh, Hydrol. Earth Syst. Sci., 26, 5473-5491, 10.5194/hess-26-5473-2022, 2022.

Ferson, S. and Ginzburg, L. R.: Different methods are needed to propagate ignorance and variability, Reliability Engineering & System Safety, 54, 133-144, 10.1016/S0951-8320(96)00071-3, 1996.

Gallien, T. W., Kalligeris, N., Delisle, M.-P. C., Tang, B.-X., Lucey, J. T., and Winters, M. A.: Coastal flood modeling challenges in defended urban backshores, Geosciences, 8, 450, 10.3390/geosciences8120450, 2018.

Ghanbari, M., Arabi, M., Kao, S. C., Obeysekera, J., and Sweet, W.: Climate Change and Changes in Compound Coastal-Riverine Flooding Hazard Along the US Coasts, Earth's Future, 9, e2021EF002055, 10.1029/2021EF002055, 2021.

Gori, A., Lin, N., and Smith, J.: Assessing compound flooding from landfalling tropical cyclones on the North Carolina coast, Water Resources Research, 56, e2019WR026788, 10.1029/2019WR026788, 2020.

Gori, A. and Lin, N.: Projecting compound flood hazard under climate change with physical models and joint probability methods, Earth's Future, e2022EF003097, 2022.

Grimaldi, S. and Serinaldi, F.: Asymmetric copula in multivariate flood frequency analysis, Advances in Water Resources, 29, 1155-1167, 10.1016/j.advwatres.2005.09.005, 2006.

Guo, A., Chang, J., Wang, Y., Huang, Q., and Li, Y.: Uncertainty quantification and propagation in bivariate design flood estimation using a Bayesian information-theoretic approach, Journal of Hydrology, 584, 124677, 10.1016/j.jhydrol.2020.124677, 2020.

Gupta, H. V., Kling, H., Yilmaz, K. K., and Martinez, G. F.: Decomposition of the mean squared error and NSE performance criteria: Implications for improving hydrological modelling, Journal of hydrology, 377, 80-91, 10.1016/j.jhydrol.2009.08.003, 2009.

Hall, J. W.: Handling uncertainty in the hydroinformatic process, Journal of Hydroinformatics, 5, 215-232, 10.2166/hydro.2003.0019, 2003.

© Author(s) 2023. CC BY 4.0 License.

Hanson, S., Nicholls, R., Ranger, N., Hallegatte, S., Corfee-Morlot, J., Herweijer, C., and Chateau, J.: A global ranking of port cities with high exposure to climate extremes, Climatic change, 104, 89-111, 10.1007/s10584-010-9977-4, 2011.

Hendry, A., Haigh, I. D., Nicholls, R. J., Winter, H., Neal, R., Wahl, T., Joly-Laugel, A., and Darby, S. E.: Assessing the characteristics and drivers of compound flooding events around the UK coast, Hydrology and Earth System Sciences, 23, 3117-3139, 10.5194/hess-23-3117-2019, 2019.

Hersbach, H., de Rosnay, P., Bell, B., Schepers, D., Simmons, A., Soci, C., Abdalla, S., Alonso-Balmaseda, M., Balsamo, G., and Bechtold, P.: Operational global reanalysis: progress, future directions and synergies with NWP, 10.21957/tkic6g3wm, 2018.

Hinkel, J., Lincke, D., Vafeidis, A. T., Perrette, M., Nicholls, R. J., Tol, R. S., Marzeion, B., Fettweis, X., Ionescu, C., and Levermann, A.: Coastal flood damage and adaptation costs under 21st century sea-level rise, Proceedings of the National Academy of Sciences, 111, 3292-3297, 10.1073/pnas.1222469111, 2014.

Hodges, B. R.: Challenges in continental river dynamics, Environmental modelling & software, 50, 16-20, 10.1016/j.envsoft.2013.08.010, 2013.

Ikeuchi, H., Hirabayashi, Y., Yamazaki, D., Muis, S., Ward, P. J., Winsemius, H. C., Verlaan, M., and Kanae, S.: Compound simulation of fluvial floods and storm surges in a global coupled river-coast flood model: Model development and its application to 2007 C yclone S idr in B angladesh, Journal of Advances in Modeling Earth Systems, 9, 1847-1862, 10.1002/2017MS000943, 2017.

Judi, D. R., Rakowski, C. L., Waichler, S. R., Feng, Y., and Wigmosta, M. S.: Integrated modeling approach for the development of climate-informed, actionable information, Water, 10, 775, 10.3390/w10060775, 2018.

Kalyanapu, A. J., Judi, D. R., McPherson, T. N., and Burian, S. J.: Annualised risk analysis approach to recommend appropriate level of flood control: application to S wannanoa river watershed, Journal of Flood Risk Management, 8, 368-385, 10.1111/jfr3.12108, 2015.

Kendall, M. G.: A new measure of rank correlation, Biometrika, 30, 81-93, 10.2307/2332226, 1938.

Kew, S., Selten, F., Lenderink, G., and Hazeleger, W.: The simultaneous occurrence of surge and discharge extremes for the Rhine delta, Natural Hazards and Earth System Sciences, 13, 2017-2029, 10.5194/nhess-13-2017-2013, 2013.

Kiang, J. E., Gazoorian, C., McMillan, H., Coxon, G., Le Coz, J., Westerberg, I. K., Belleville, A., Sevrez, D., Sikorska, A. E., and Petersen-Øverleir, A.: A comparison of methods for streamflow uncertainty estimation, Water Resources Research, 54, 7149-7176, 10.1029/2018WR022708, 2018.

Kojadinovic, I. and Yan, J.: Modeling multivariate distributions with continuous margins using the copula R package, Journal of Statistical Software, 34, 1-20, 10.18637/jss.v034.i09, 2010.

Kron, W.: Flood risk= hazard• values• vulnerability, Water international, 30, 58-68, 10.1080/02508060508691837, 2005.

Kulp, S. A. and Strauss, B. H.: New elevation data triple estimates of global vulnerability to sea-level rise and coastal flooding, Nature communications, 10, 1-12, s41467-019-12808-z, 2019.

© Author(s) 2023. CC BY 4.0 License.

Kumbier, K., Carvalho, R. C., Vafeidis, A. T., and Woodroffe, C. D.: Investigating compound flooding in an estuary using hydrodynamic modelling: a case study from the Shoalhaven River, Australia, Natural Hazards and Earth System Sciences, 18, 463-477, 10.5194/nhess-18-463-2018, 2018.

Lamb, M. P., Nittrouer, J. A., Mohrig, D., and Shaw, J.: Backwater and river plume controls on scour upstream of river mouths: Implications for fluvio-deltaic morphodynamics, Journal of Geophysical Research: Earth Surface, 117, 10.1029/2011JF002079, 2012.

Lehner, B. and Grill, G.: Global river hydrography and network routing: baseline data and new approaches to study the world's large river systems, Hydrological Processes, 27, 2171-2186, 10.1002/hyp.9740, 2013.

Lehner, B., Verdin, K., and Jarvis, A.: New global hydrography derived from spaceborne elevation data, Eos, Transactions American Geophysical Union, 89, 93-94, 10.1029/2008EO100001, 2008.

Li, H., Wigmosta, M. S., Wu, H., Huang, M., Ke, Y., Coleman, A. M., and Leung, L. R.: A physically based runoff routing model for land surface and earth system models, Journal of Hydrometeorology, 14, 808-828, 10.1175/JHM-D-12-015.1, 2013.

Li, H.-Y., Tan, Z., Ma, H., Zhu, Z., Abeshu, G. W., Zhu, S., Cohen, S., Zhou, T., Xu, D., and Leung, L. R.: A new large-scale suspended sediment model and its application over the United States, Hydrology and Earth System Sciences, 26, 665-688, 10.5194/hess-26-665-2022, 2022.

Lian, J., Xu, K., and Ma, C.: Joint impact of rainfall and tidal level on flood risk in a coastal city with a complex river network: a case study of Fuzhou City, China, Hydrology and Earth System Sciences, 17, 679-689, 10.5194/hess-17-679-2013, 2013.

Luo, X., Li, H.-Y., Leung, L. R., Tesfa, T. K., Getirana, A., Papa, F., and Hess, L. L.: Modeling surface water dynamics in the Amazon Basin using MOSART-Inundation v1. 0: impacts of geomorphological parameters and river flow representation, Geoscientific Model Development, 10, 1233-1259, 10.5194/gmd-10-1233-2017, 2017.

Maskrey, A., Peduzzi, P., Chatenoux, B., Herold, C., Dao, Q.-H., and Giuliani, G.: Revealing Risk, Redefining Development, Global Assessment Report on Disaster Risk Reduction, United Nations Strategy for Disaster Reduction, 17-51, 2011.

Mehran, A., AghaKouchak, A., Nakhjiri, N., Stewardson, M. J., Peel, M. C., Phillips, T. J., Wada, Y., and Ravalico, J. K.: Compounding impacts of human-induced water stress and climate change on water availability, Scientific Reports, 7, 1-9, s41598-017-06765-0, 2017.

Moftakhari, H., Schubert, J. E., AghaKouchak, A., Matthew, R. A., and Sanders, B. F.: Linking statistical and hydrodynamic modeling for compound flood hazard assessment in tidal channels and estuaries, Advances in Water Resources, 128, 28-38, 10.1016/j.advwatres.2019.04.009, 2019.

Moftakhari, H. R., Salvadori, G., AghaKouchak, A., Sanders, B. F., and Matthew, R. A.: Compounding effects of sea level rise and fluvial flooding, Proceedings of the National Academy of Sciences, 114, 9785-9790, 10.1073/pnas.1620325114, 2017.

Muis, S., Apecechea, M. I., Dullaart, J., de Lima Rego, J., Madsen, K. S., Su, J., Yan, K., and Verlaan, M.: A high-resolution global dataset of extreme sea levels, tides, and storm surges, including future projections, Frontiers in Marine Science, 7, 263, 10.3389/fmars.2020.00263, 2020.

Muis, S., Apecechea, M. I., Álvarez, J. A., Verlaan, M., Yan, K., Dullaart, J., Aerts, J., Duong, T., Ranasinghe, R., Erikson, L., O'Neill, A., Bars, D. l., Haarsma, R., and Roberts, M.: Global sea level change time series from 1950 to 2050 derived from reanalysis and high resolution CMIP6 climate projections., 10.24381/cds.a6d42d60, 2022.

Muis, S., Verlaan, M., Nicholls, R. J., Brown, S., Hinkel, J., Lincke, D., Vafeidis, A. T., Scussolini, P., Winsemius, H. C., and Ward, P. J.: A comparison of two global datasets of extreme sea levels and resulting flood exposure, Earth's Future, 5, 379-392, 10.1002/2016EF000430, 2017.

Muñoz, D., Moftakhari, H., and Moradkhani, H.: Compound effects of flood drivers and wetland elevation correction on coastal flood hazard assessment, Water Resources Research, 56, e2020WR027544, 10.1029/2020WR027544, 2020.

Nasr, A. A., Wahl, T., Rashid, M. M., Camus, P., and Haigh, I. D.: Assessing the dependence structure between oceanographic, fluvial, and pluvial flooding drivers along the United States coastline, Hydrology and Earth System Sciences, 25, 6203-6222, 10.5194/hess-2021-268, 2021.

Neal, J., Villanueva, I., Wright, N., Willis, T., Fewtrell, T., and Bates, P.: How much physical complexity is needed to model flood inundation?, Hydrological Processes, 26, 2264-2282, 10.1002/hyp.8339, 2012.

NOAA: NOAA tides & currents, https://tidesandcurrents.noaa.gov/, last access: 19 January 2023.

Olbert, A. I., Comer, J., Nash, S., and Hartnett, M.: High-resolution multi-scale modelling of coastal flooding due to tides, storm surges and rivers inflows. A Cork City example, Coastal Engineering, 121, 278-296, 10.1016/j.coastaleng.2016.12.006, 2017.

Paprotny, D., Vousdoukas, M. I., Morales-Nápoles, O., Jonkman, S. N., and Feyen, L.: Pan-European hydrodynamic models and their ability to identify compound floods, Natural Hazards, 101, 933-957, 10.1007/s11069-020-03902-3, 2020.

Parodi, M. U., Giardino, A., Van Dongeren, A., Pearson, S. G., Bricker, J. D., and Reniers, A. J.: Uncertainties in coastal flood risk assessments in small island developing states, Natural Hazards and Earth System Sciences, 20, 2397-2414, 10.5194/nhess-20-2397-2020, 2020.

Phongsapan, K., Chishtie, F., Poortinga, A., Bhandari, B., Meechaiya, C., Kunlamai, T., Aung, K. S., Saah, D., Anderson, E., and Markert, K.: Operational flood risk index mapping for disaster risk reduction using Earth Observations and cloud computing technologies: a case study on Myanmar, Frontiers in Environmental Science, 7, 191, 10.3389/fenvs.2019.00191, 2019.

Pörtner, H.-O., Roberts, D. C., Masson-Delmotte, V., Zhai, P., Tignor, M., Poloczanska, E., and Weyer, N.: The ocean and cryosphere in a changing climate, IPCC Special Report on the Ocean and Cryosphere in a Changing Climate, 10.1017/9781009157964, 2019.

Rashid, M., Wahl, T., Chambers, D. P., Calafat, F. M., and Sweet, W. V.: An extreme sea level indicator for the contiguous United States coastline, Scientific Data, 6, 1-14, 10.1038/s41597-019-0333-x, 2019.

https://doi.org/10.5194/hess-2023-31
Preprint. Discussion started: 2 February 2023
© Author(s) 2023. CC BY 4.0 License.

Sadegh, M., Moftakhari, H., Gupta, H. V., Ragno, E., Mazdiyasni, O., Sanders, B., Matthew, R., and AghaKouchak, A.: Multihazard scenarios for analysis of compound extreme events, Geophysical Research Letters, 45, 5470-5480, 10.1029/2018GL077317, 2018.

Sadegh, M., Ragno, E., and AghaKouchak, A.: Multivariate C opula A nalysis T oolbox (MvCAT): describing dependence and underlying uncertainty using a B ayesian framework, Water Resources Research, 53, 5166-5183, 10.1002/2016WR020242, 2017.

Salvadori, G., De Michele, C., Kottegoda, N. T., and Rosso, R.: Extremes in nature: an approach using copulas, Springer Science & Business Media, 2007.

Salvadori, G., Durante, F., De Michele, C., Bernardi, M., and Petrella, L.: A multivariate copula-based framework for dealing with hazard scenarios and failure probabilities, Water Resources Research, 52, 3701-3721, 10.1002/2015WR017225, 2016.

Santiago-Collazo, F. L., Bilskie, M. V., and Hagen, S. C.: A comprehensive review of compound inundation models in low-gradient coastal watersheds, Environmental Modelling & Software, 119, 166-181, 10.1016/j.envsoft.2019.06.002, 2019.

Schiavina, M., Freire, S., and MacManus, K.: GHS population grid multitemporal (1975, 1990, 2000, 2015) R2019A, European Commission, Joint Research Centre (JRC), 10, 10.2905/42E8BE89-54FF-464E-BE7B-BF9E64DA5218, 2019.

Seneviratne, S., Nicholls, N., Easterling, D., Goodess, C., Kanae, S., Kossin, J., Luo, Y., Marengo, J., McInnes, K., and Rahimi, M.: Changes in climate extremes and their impacts on the natural physical environment, 10.7916/d8-6nbt-s431, 2012.

Serafin, K. A., Ruggiero, P., Parker, K., and Hill, D. F.: What's streamflow got to do with it? A probabilistic simulation of the competing oceanographic and fluvial processes driving extreme along-river water levels, Natural Hazards and Earth System Sciences, 19, 1415-1431, 10.5194/nhess-19-1415-2019, 2019, 2019.

Sun, N., Wigmosta, M. S., Judi, D., Yang, Z., Xiao, Z., and Wang, T.: Climatological analysis of tropical cyclone impacts on hydrological extremes in the Mid-Atlantic region of the United States, Environmental Research Letters, 16, 124009, 10.1088/1748-9326/ac2d6a, 2021.

Towner, J., Cloke, H. L., Zsoter, E., Flamig, Z., Hoch, J. M., Bazo, J., Coughlan de Perez, E., and Stephens, E. M.: Assessing the performance of global hydrological models for capturing peak river flows in the Amazon basin, Hydrology and Earth System Sciences, 23, 3057-3080, 10.5194/hess-23-3057-2019, 2019.

Turnipseed, D. P. and Sauer, V. B.: Discharge measurements at gaging stations, US Geological Survey2328-7055, 10.3133/tm3A8, 2010.

U.S. Geological Survey: National Water Information System data available on the World Wide Web (USGS Water Data for the Nation), http://waterdata.usgs.gov/nwis/ (last access: 19 January 2023), 2016.

U.S. Geological Survey: USGS 3D Elevation Program Digital Elevation Model, https://elevation.nationalmap.gov/arcgis/rest/services/3DEPElevation/ImageServer (last access: 19 January 2023), 2019.

© Author(s) 2023. CC BY 4.0 License.

Uusitalo, L., Lehikoinen, A., Helle, I., and Myrberg, K.: An overview of methods to evaluate uncertainty of deterministic models in decision support, Environmental Modelling & Software, 63, 24-31, 10.1016/j.envsoft.2014.09.017, 2015.

Valle-Levinson, A., Olabarrieta, M., and Heilman, L.: Compound flooding in Houston-Galveston Bay during Hurricane Harvey, Science of the Total Environment, 747, 141272, 10.1016/j.scitotenv.2020.141272, 2020.

Van de Sande, B., Lansen, J., and Hoyng, C.: Sensitivity of coastal flood risk assessments to digital elevation models, Water, 4, 568-579, 10.3390/w4030568, 2012.

Vousdoukas, M. I., Bouziotas, D., Giardino, A., Bouwer, L. M., Mentaschi, L., Voukouvalas, E., and Feyen, L.: Understanding epistemic uncertainty in large-scale coastal flood risk assessment for present and future climates, Natural Hazards and Earth System Sciences, 18, 2127-2142, 10.5194/nhess-18-2127-2018, 2018.

Wahl, T., Haigh, I. D., Nicholls, R. J., Arns, A., Dangendorf, S., Hinkel, J., and Slangen, A. B.: Understanding extreme sea levels for broad-scale coastal impact and adaptation analysis, Nature communications, 8, 1-12, 10.1038/ncomms16075, 2017.

Wahl, T., Jain, S., Bender, J., Meyers, S. D., and Luther, M. E.: Increasing risk of compound flooding from storm surge and rainfall for major US cities, Nature Climate Change, 5, 1093-1097, 10.1038/NCLIMATE2736, 2015.

Ward, P. J., Couasnon, A., Eilander, D., Haigh, I. D., Hendry, A., Muis, S., Veldkamp, T. I., Winsemius, H. C., and Wahl, T.: Dependence between high sea-level and high river discharge increases flood hazard in global deltas and estuaries, Environmental Research Letters, 13, 084012, 10.1088/1748-9326/aad400, 2018.

Woolway, R. I., Sharma, S., Weyhenmeyer, G. A., Debolskiy, A., Golub, M., Mercado-Bettín, D., Perroud, M., Stepanenko, V., Tan, Z., and Grant, L.: Phenological shifts in lake stratification under climate change, Nature communications, 12, 1-11, 10.1038/s41467-021-22657-4, 2021.

Wu, W., Westra, S., and Leonard, M.: Estimating the probability of compound floods in estuarine regions, Hydrology and Earth System Sciences, 25, 2821-2841, 10.5194/hess-25-2821-2021, 2021.

Xiao, Z., Yang, Z., Wang, T., Sun, N., Wigmosta, M., and Judi, D.: Characterizing the non-linear interactions between tide, storm surge, and river flow in the delaware bay estuary, United States, Front. Mar. Sci., 8, 715557, 10.3389/fmars.2021.715557, 2021.

Xu, D., Bisht, G., Zhou, T., Leung, L. R., and Pan, M.: Development of Land-River Two-Way Hydrologic Coupling for Floodplain Inundation in the Energy Exascale Earth System Model, Journal of Advances in Modeling Earth Systems, 14, e2021MS002772, 10.1029/2021MS002772, 2022.

Xu, K., Wang, C., and Bin, L.: Compound flood models in coastal areas: a review of methods and uncertainty analysis, Natural Hazards, 1-28, 10.1007/s11069-022-05683-3, 2022.

Yamazaki, D., Lee, H., Alsdorf, D. E., Dutra, E., Kim, H., Kanae, S., and Oki, T.: Analysis of the water level dynamics simulated by a global river model: A case study in the Amazon River, Water Resources Research, 48, 10.1029/2012WR011869, 2012.

https://doi.org/10.5194/hess-2023-31
Preprint. Discussion started: 2 February 2023
© Author(s) 2023. CC BY 4.0 License.
Hydrology and Earth System Sciences
Open Access
EGU
Discussions

Yan, K., Muis, S., Irazoqui Apecechea, M. and Verlaan, M.: Water level change time series for the European coast from 1977 to 2100 derived from climate projections. Copernicus Climate Change Service (C3S) Climate Data Store (CDS), (last access: 19 January 2023), 10.24381/cds.8c59054f, 2022

Yang, Y., Pan, M., Lin, P., Beck, H. E., Zeng, Z., Yamazaki, D., David, C. H., Lu, H., Yang, K., and Hong, Y.: Global Reach-Level 3-Hourly River Flood Reanalysis (1980–2019), Bulletin of the American Meteorological Society, 102, E2086-E2105, 10.1175/BAMS-D-20-0057.1, 2021.

Ye, F., Zhang, Y. J., Yu, H., Sun, W., Moghimi, S., Myers, E., Nunez, K., Zhang, R., Wang, H. V., and Roland, A.: Simulating storm surge and compound flooding events with a creek-to-ocean model: Importance of baroclinic effects, Ocean Modelling, 145, 101526, 10.1016/j.ocemod.2019.101526, 2020.

Zhang, D., Shi, X., Xu, H., Jing, Q., Pan, X., Liu, T., Wang, H., and Hou, H.: A GIS-based spatial multi-index model for flood risk assessment in the Yangtze River Basin, China, Environmental Impact Assessment Review, 83, 106397, 10.1016/j.eiar.2020.106397, 2020.

Zhang, Y. J., Ye, F., Yu, H., Sun, W., Moghimi, S., Myers, E., Nunez, K., Zhang, R., Wang, H., and Roland, A.: Simulating compound flooding events in a hurricane, Ocean Dynamics, 70, 621-640, 10.1007/s10236-020-01351-x, 2020.

Zscheischler, J., Martius, O., Westra, S., Bevacqua, E., Raymond, C., Horton, R. M., van den Hurk, B., AghaKouchak, A., Jézéquel, A., and Mahecha, M. D.: A typology of compound weather and climate events, Nature reviews earth & environment, 1, 333-347, 10.1038/s43017-020-0060-z, 2020.

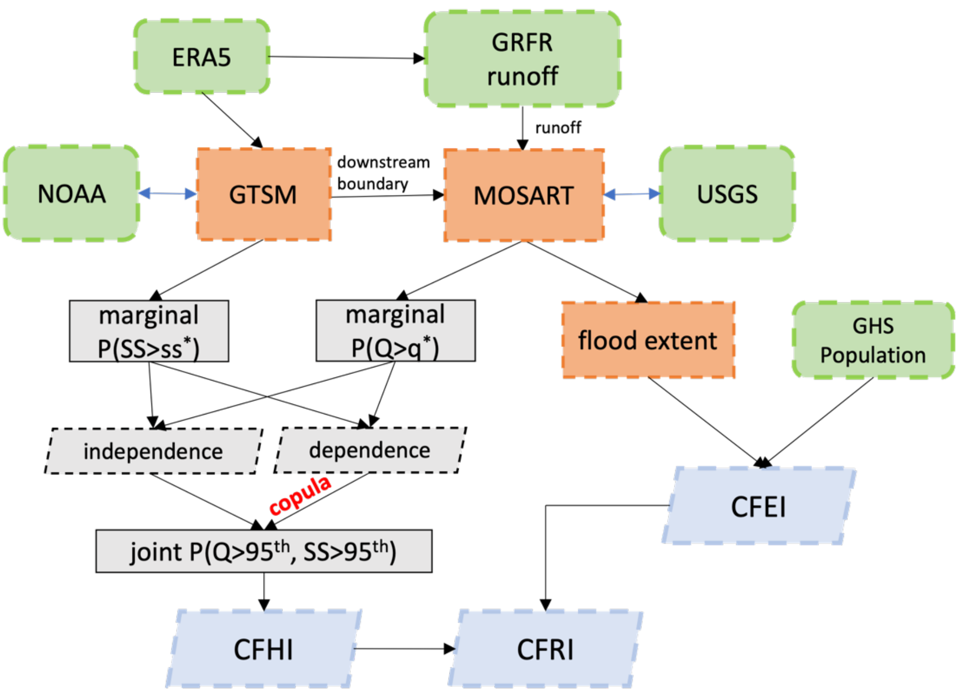

https://doi.org/10.5194/hess-2023-31
Preprint. Discussion started: 2 February 2023
© Author(s) 2023. CC BY 4.0 License.
Hydrology and Earth System Sciences
Open Access
Discussions

Figure 1: The CFRA framework. Data, numerical modeling, statistical modeling, and risk calculation are represented by green, orange, gray, and blue colors, respectively.

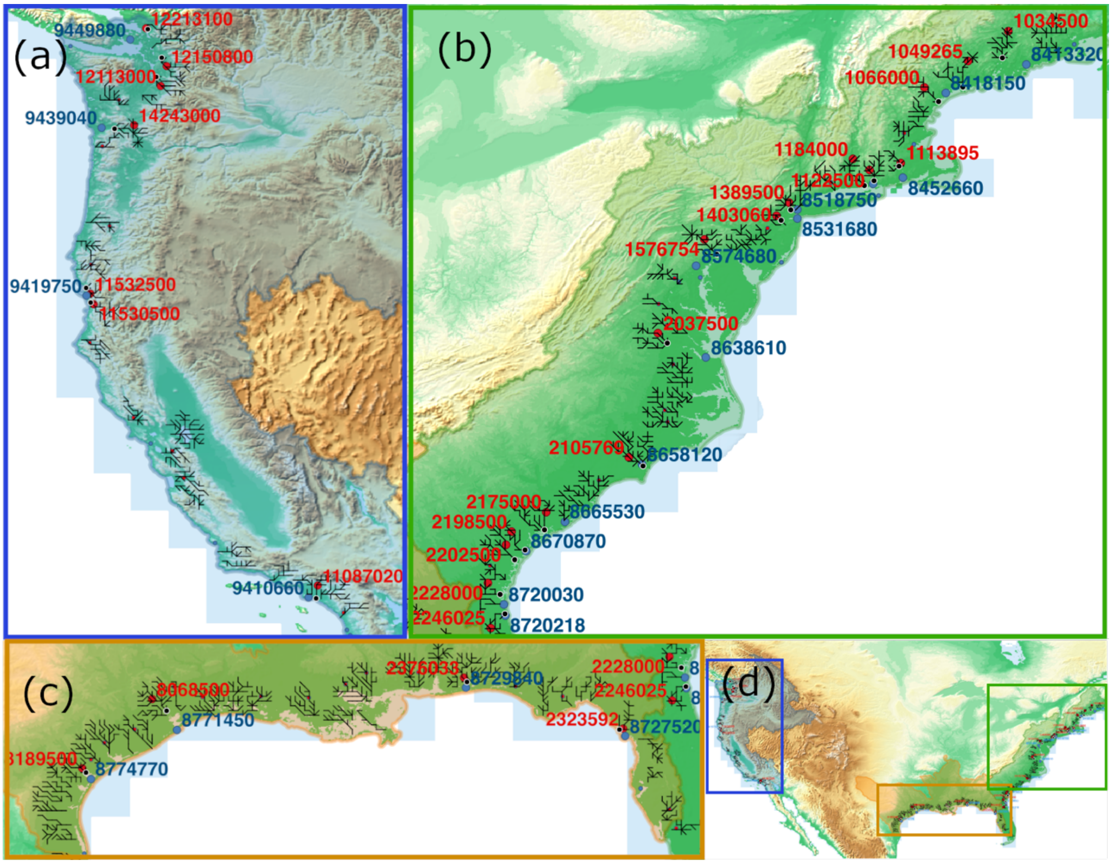

Figure 2: Study domain and observations overlaid on the USGS 3D elevation. The map is created using the free and open source QGIS on the USGS 3D Elevation Program (3DEP) Hillshade elevation map (U.S. Geological Survey, 2019). The red and blue circles represent the USGS and NOAA gauges, respectively. The gauges used for identifying uncertainties are labeled with the gauge ID. The black solid lines are the coastal river network that consists of at most seven cells from each river outlet.

https://doi.org/10.5194/hess-2023-31
Preprint. Discussion started: 2 February 2023
© Author(s) 2023. CC BY 4.0 License.

Hydrology and Earth System Sciences
Open Access
EGU
Discussions

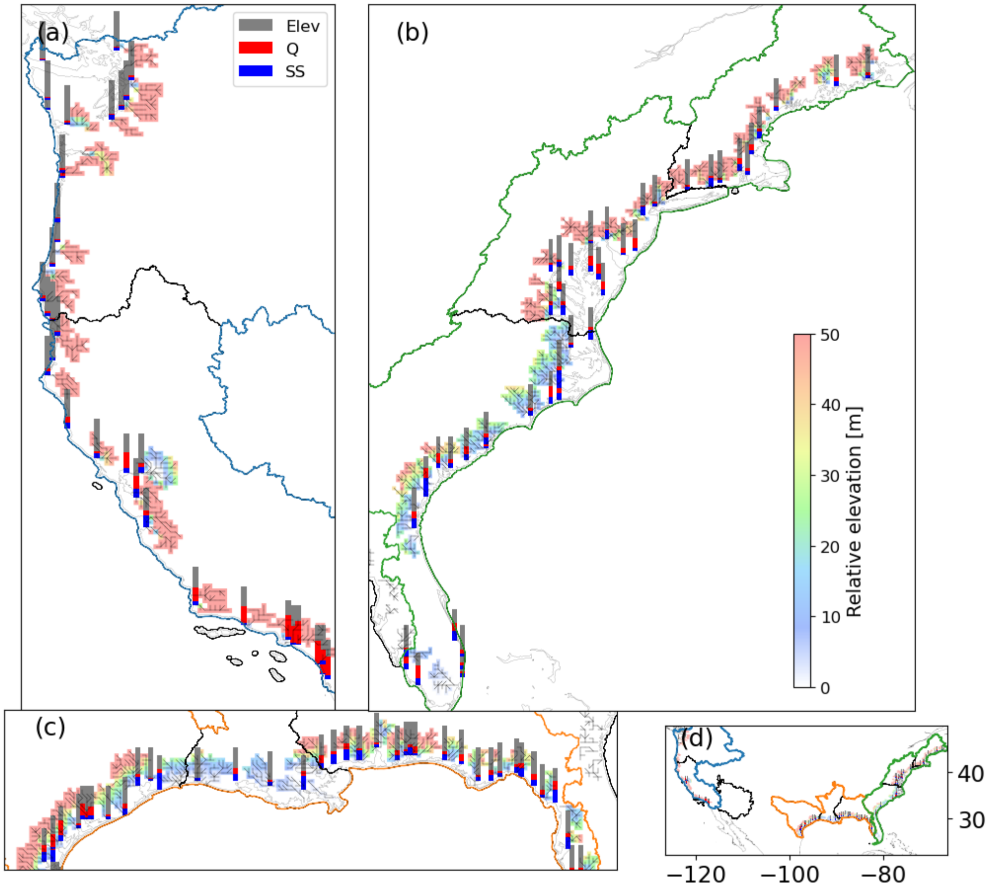

725 **Figure 3: The relative importance of *Q* (red), *SS* (blue) and relative riverbed elevation (gray) along the (a) West coast, (b) East coast, (c) CONUS, and (d) Gulf coast. The river networks within the MOSART coastal cells are presented using black solid lines.**

Hydrology and Earth System Sciences
Discussions

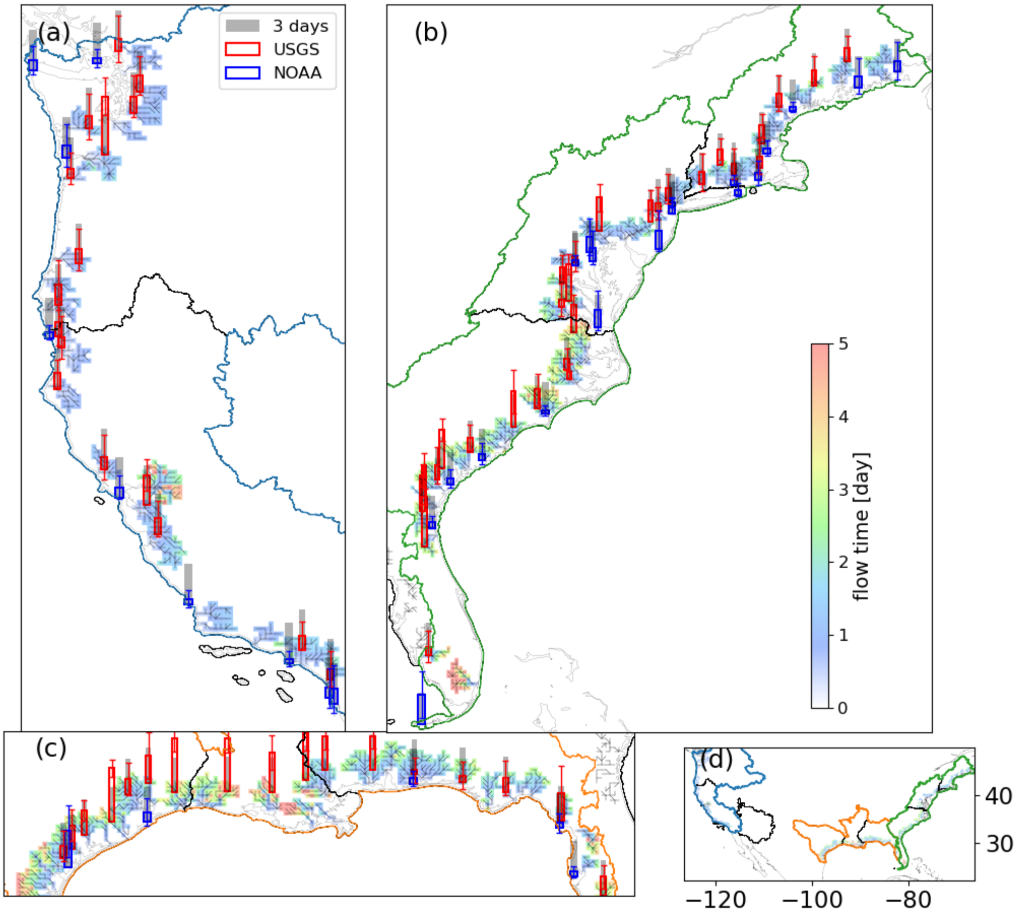

Figure 4: The flow time at the MOSART coastal cells and the shifted days in the *Q* and *SS* peaks between the observation gauges and the corresponding river outlets along the (a) West coast, (b) East coast, (c) CONUS, and (d) Gulf coast. The rectangular box represents the averaged shift over the simulation period and the error bar represents the standard deviation. The gray box is used as a reference of 3 days for comparison.

https://doi.org/10.5194/hess-2023-31
Preprint. Discussion started: 2 February 2023
© Author(s) 2023. CC BY 4.0 License.
Hydrology and Earth System Sciences
Discussions

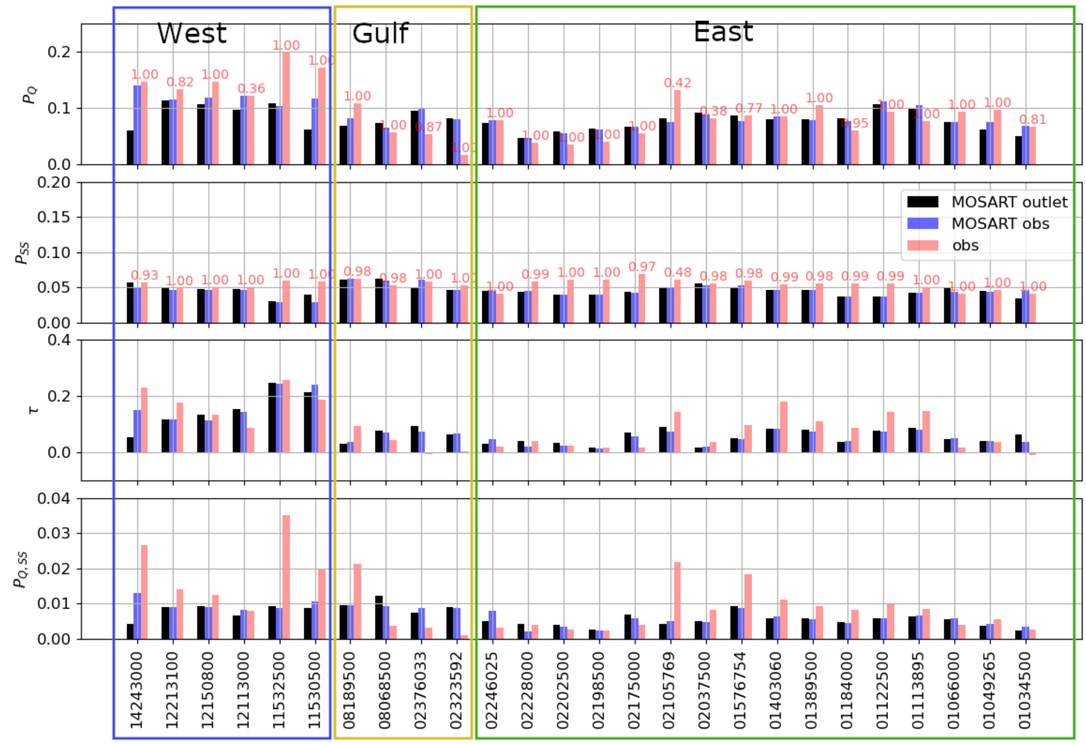

Figure 5: The comparison of P_Q, P_{SS}, τ and $P_{Q,SS}$ computed from the modeled Q and SS at the river outlet (black), modeled Q and SS at the observation gauges (blue), measured Q and SS at the observation gauges (pink). The number on top of each bar is the percentage of the data coverage.

https://doi.org/10.5194/hess-2023-31
Preprint. Discussion started: 2 February 2023
© Author(s) 2023. CC BY 4.0 License.

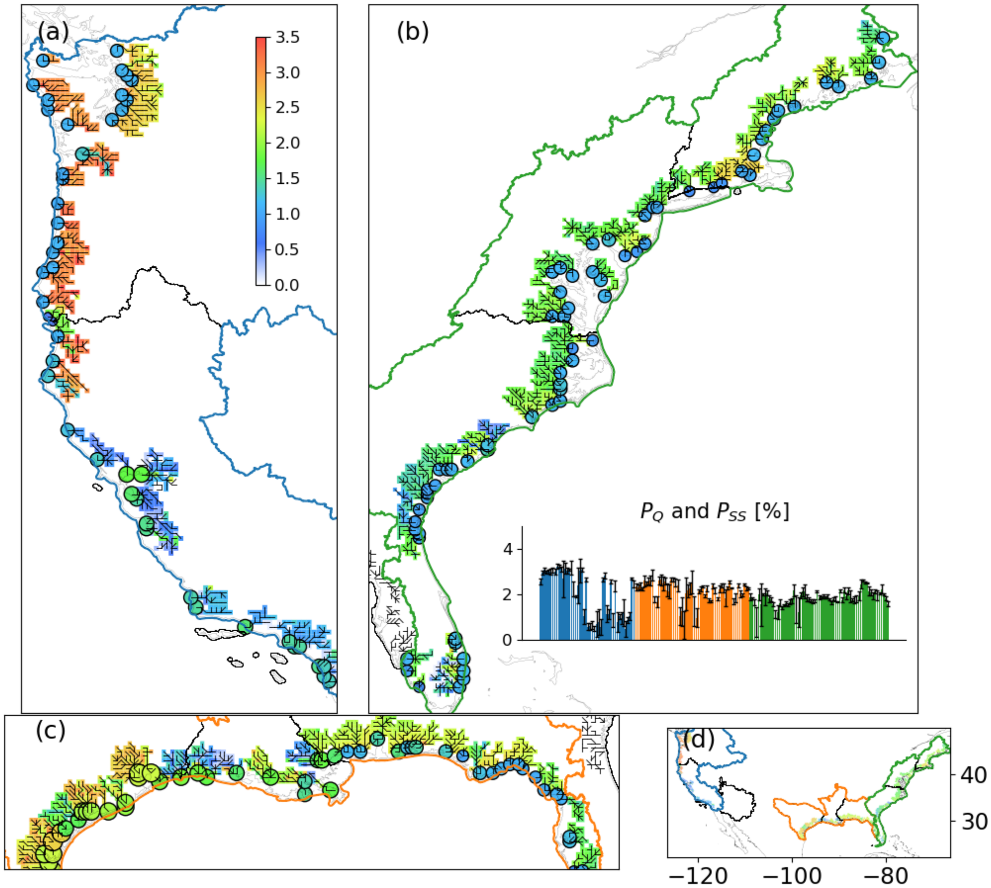

740 **Figure 6: The marginal exceedance probability P_Q is represented by the contour map and P_{SS} is represented by the colored circles located at the GTSM cells nearest to the corresponding outlets. The basin-averaged P_Q is provided in the counter-clockwise order of the basins along the US coast in the lower left subplot of (b) where the error bars represent the standard deviation of P_Q in each basin.**

https://doi.org/10.5194/hess-2023-31
Preprint. Discussion started: 2 February 2023
© Author(s) 2023. CC BY 4.0 License.

Hydrology and Earth System Sciences
Discussions

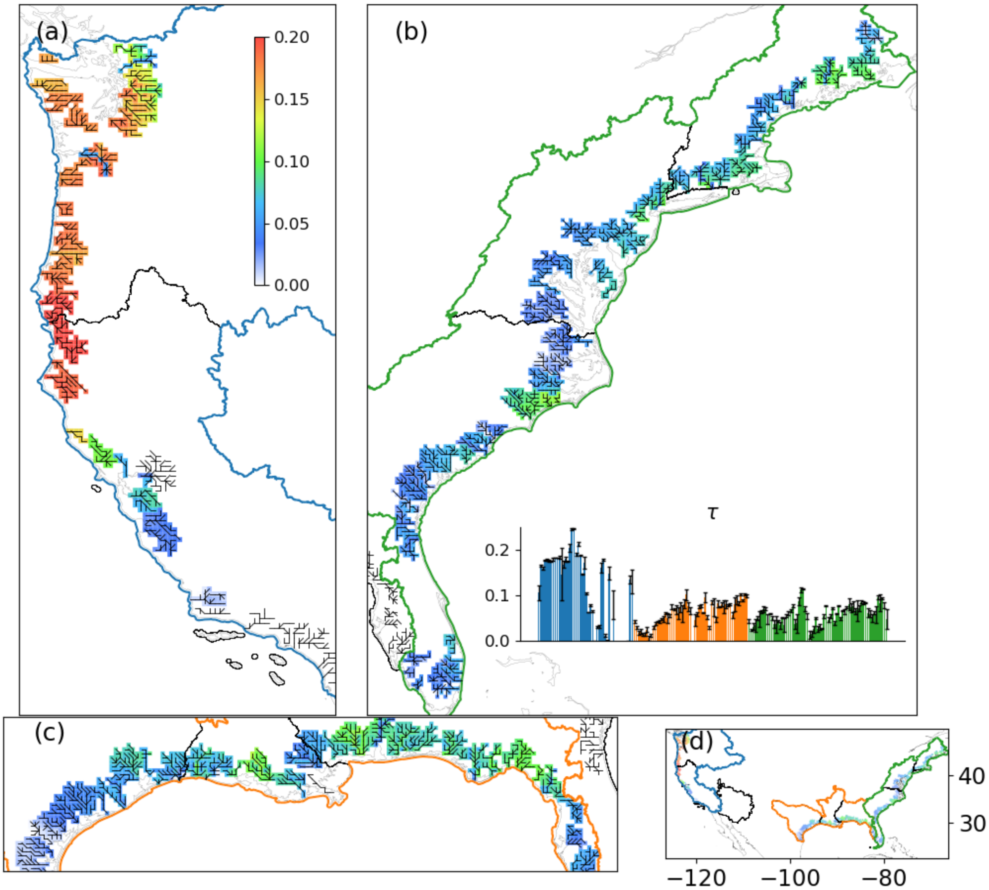

Figure 7: The Kendall's correlation coefficient (τ). The subplot in (b) is the basin-averaged τ with each error bar representing the standard deviation.

https://doi.org/10.5194/hess-2023-31
Preprint. Discussion started: 2 February 2023
© Author(s) 2023. CC BY 4.0 License.

Hydrology and Earth System Sciences
Discussions

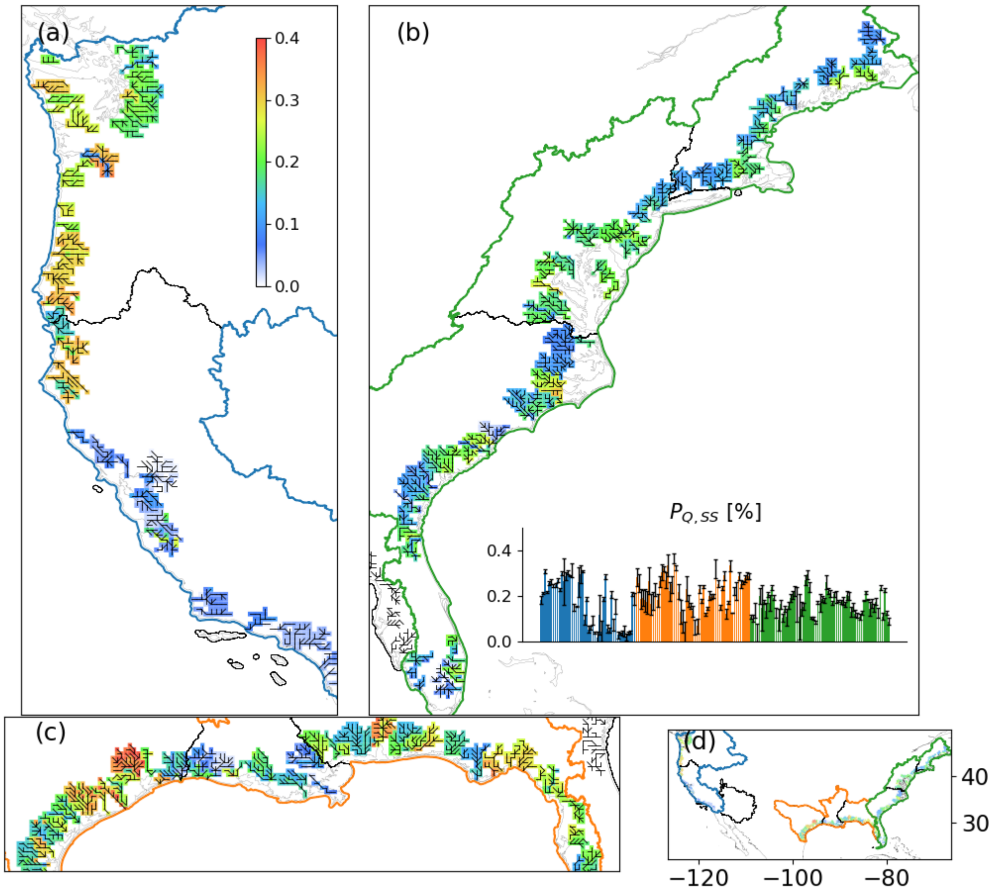

745 **Figure 8: The joint exceedance probability ($P_{Q,SS}$). The subplot in (b) is the basin-averaged $P_{Q,SS}$ with each error bar representing the standard deviation.**

https://doi.org/10.5194/hess-2023-31
Preprint. Discussion started: 2 February 2023
© Author(s) 2023. CC BY 4.0 License.

Hydrology and Earth System Sciences
Open Access
EGU
Discussions

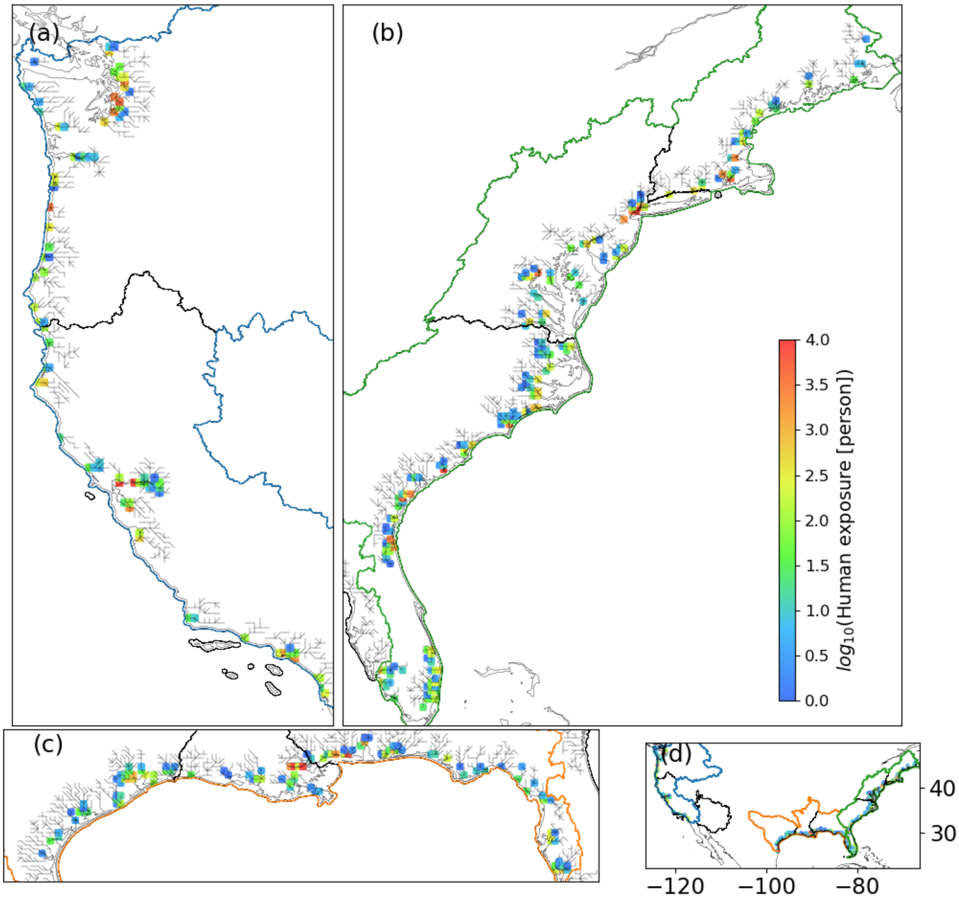

Figure 9: The accumulated population exposed to CF over the simulation period.

Hydrology and Earth System Sciences
Open Access
Discussions

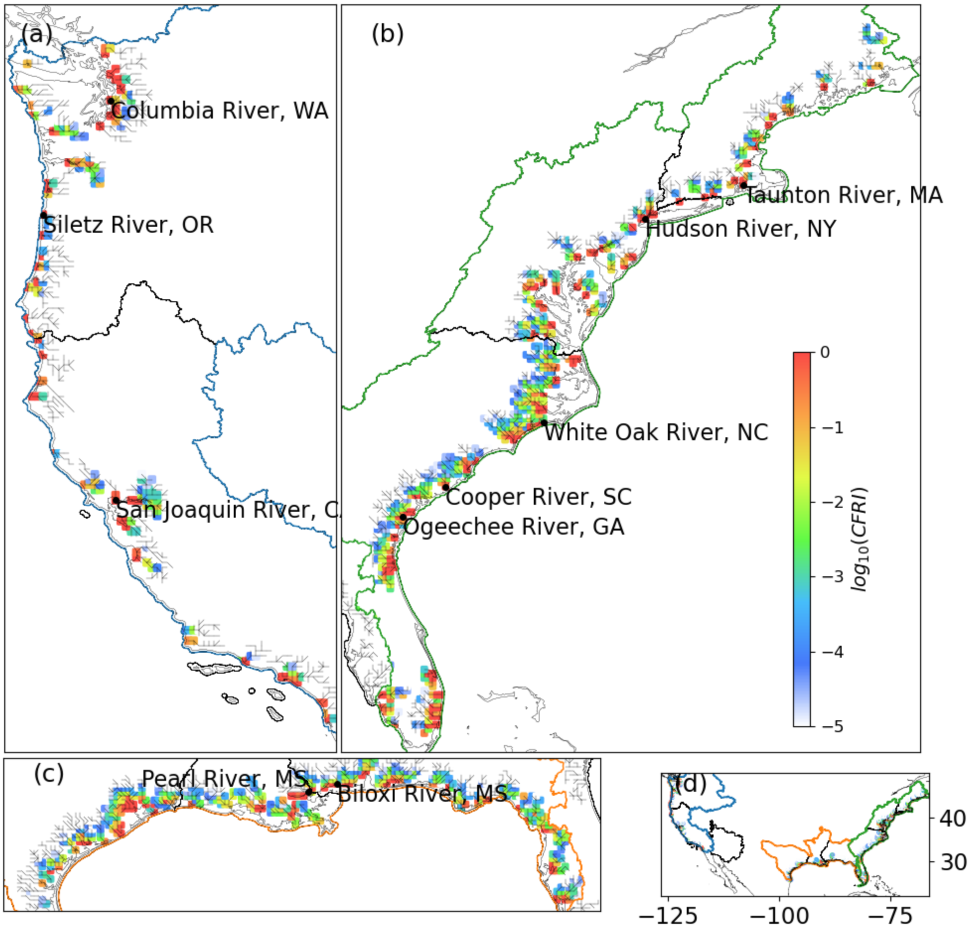

Figure 10: The CF comprehensive risk (CFRI) along the CONUS coast.

https://doi.org/10.5194/hess-2023-31
Preprint. Discussion started: 2 February 2023
© Author(s) 2023. CC BY 4.0 License.

Table 1: Uncertainty sources in CFRA. Sources in boldfaces are considered in the analysis.

Module	Aleatory uncertainty	Epistemic uncertainty
Statistical models	**Spatial variability in fluvial processes and river topology**	**Measurement uncertainty (e.g., measurement errors, inappropriate in-situ locations, and limited data coverage or partial time series)**
	Non-stationarity	Model structure uncertainty (e.g., selection of probability distribution functions and selection of dependence models)
Numerical models	Future climate change	Parameter uncertainty
		Data uncertainty (e.g., uncertain river topology and channel geometry data)
		Model structure uncertainty (e.g., simplified flood wave physics, uncertain runoff generation schemes, and coarse spatial resolutions)

Table 2: Top ten rivers with high CF risk. The locations are shown in Figure 10. CFRI represents the averaged CF comprehensive risk index (Eq (7)) in the river basin. Population exposure is the total population exposed to CF over the simulation period.

No.	River name	River outlet Location	CFRI	Population exposure [person]	Maximum CF probability (%)
1	Ogeechee River, GA	31.9375, -81.1875	38.617	4,617	0.158
2	Cooper River, SC	32.8125, -79.9375	36.468	11,096	0.264
3	San Joaquin River, CA	38.0625, -122.3125	33.182	19,621	0.075
4	Pearl River, MS	30.1875, -89.8125	19.829	103,314	0.131
5	Hudson River, NY	40.6875, -74.0625	19.516	22,542	0.151

© Author(s) 2023. CC BY 4.0 License.

6	White Oak River, NC	34.6875, -77.0625	19.076	1,849	0.283
7	Biloxi River, MS	30.4375, -88.9375	12.414	2,261	0.253
8	Siletz River, OR	44.9375, -124.0625	11.467	2,438	0.278
9	Columbia River, WA	47.6875, -122.4375	10.323	1,567	0.310
10	Taunton River, MA	41.6875, -71.1875	9.528	3,795	0.186